Microbial population dynamics decouple nutrient affinity from environmental concentration

Justus Wilhelm Fink*
Institute of Integrative Biology, Department of Environmental Systems Science, ETH Zurich, Zurich, Switzerland

Noelle A. Held
Institute of Biogeochemistry and Pollutant Dynamics, Department of Environmental Systems Science, ETH Zurich, Zurich, Switzerland and Department of Environmental Microbiology, Swiss Federal Institute of Aquatic Science and Technology (Eawag), Dübendorf, Switzerland

Michael Manhart†
Institute of Integrative Biology, Department of Environmental Systems Science, ETH Zurich, Zurich, Switzerland Department of Environmental Microbiology, Swiss Federal Institute of Aquatic Science and Technology (Eawag), Dübendorf, Switzerland and Center for Advanced Biotechnology and Medicine and Department of Biochemistry and Molecular Biology, Robert Wood Johnson Medical School, Rutgers University, Piscataway, NJ, USA

(Dated: May 4, 2022)

How the growth rate of a microbial population depends on the availability of chemical nutrients and other resources in the environment is a fundamental question in microbiology. Models of this dependence, such as the well-known Monod model, are characterized by a threshold concentration (or affinity) of the resource, above which the population can grow near its maximum rate. Even though this concept is a core element of microbiological and ecological modeling, there is little empirical and theoretical evidence for the evolved diversity of these thresholds. In particular, does resource scarcity drive populations to evolve commensurately lower thresholds? To address this question, we perform the largest-to-date meta-analysis of resource threshold data across a wide range of organisms and resources, substantially expanding previous surveys. We find that the thresholds vary across orders of magnitude, even for the same organism and resource. To explain this variation, we develop an evolutionary model to show that demographic fluctuations (genetic drift) can constrain the adaptation of resource thresholds. We find that this effect fundamentally differs depending on the type of population dynamics: populations undergoing periodic bottlenecks of fixed size will adapt their thresholds in proportion to the environmental resource concentration, but populations undergoing periodic dilutions of fixed size will evolve thresholds that are largely decoupled from the environmental concentration. Our model not only provides testable predictions for laboratory evolution experiments, but it also reveals how an evolved resource threshold may not reflect the organism's environment. In particular, this explains how organisms in nutrient-rich environments can still evolve facultative growth at low resource concentrations. Altogether our results demonstrate the critical role of population dynamics in shaping fundamental ecological traits.

Keywords: Microbial evolution, Monod model, resource competition, nutrient affinity, nutrient limitation, selection-drift balance

INTRODUCTION

Microbial populations rely on a wide range of resources, including chemical nutrients such as sugars and metals, as well as space, light, and prey [1]. These resources vary in abundance or concentration across time and environments, which typically elicit differences in growth rates [2–4]. A significant literature discusses how natural populations can be classified as oligotrophs or copiotrophs [4–6], that differ, among other things, in their growth rate response to nutrient concentration. The most widely-used quantitative model of the relationship between growth rate and resource concentration is attributed to Jacques Monod [7]. In the Monod model, growth rate increases linearly with resource concentration below a threshold concentration, and then saturates at high concentrations of the resource. The threshold concentration, also sometimes known as the resource affinity, therefore plays a key role in determining the ability of the population to grow on scarce resources. This suggests that lower resource concentrations in the environment may drive populations to evolve commensurately lower thresholds [8, 9], one of the main predictions of resource-ratio theory [10–12]. Quantitative models and data for the dependence of growth rate on resource concentration are important both for predicting the behav-

* To whom correspondence should be addressed. Email: justus.fink@env.ethz.ch
† To whom correspondence should be addressed. Email: mmanhart@rutgers.edu

ior of a population under different environmental conditions [13, 14], as well as for inferring the natural environmental niche from evolved traits of the population. This inverse approach has been used, for example, to infer separate niches for ammonia-oxidizing archaea and bacteria in the global nitrogen cycle based on kinetic parameters for resource consumption [15–18].

Even though these concepts have been central elements of microbiology and ecology for decades, there is limited experimental evidence that directly demonstrates the evolution of growth rate dependence on resources. Continuous culture for 200–300 generations led to improved growth rate at low glucose concentrations for *Escherichia coli* [19, 20] and *Saccharomyces cerevisiae* [21], but these changes were not clearly attributable to genetic (rather than physiological) adaptation. The Long-Term Evolution Experiment (LTEE) of *E. coli* found that their glucose thresholds (which determine their ability to grow at low glucose concentrations) actually increased over the first 2000 generations, although the growth rates at high glucose concentrations significantly increased as well [22]. More recently, Bernhardt et al. [12] observed adaptation in the phosphorus thresholds of *Chlamydomonas reinhardtii* when limited for phosphorus, but they did not obtain consistent outcomes for nitrogen and light. Perhaps the most explicit evidence so far is from Hart et al. [23], who found that a synthetic auxotroph strain of *S. cerevisiae* significantly reduced its threshold for lysine through genetic adaptations.

While direct laboratory experiments can test the basic principle, mathematical and computational models are better suited to exploring the wide range of environments necessary to establish the link between environment and evolved traits. Previous modeling studies on this topic have focused primarily on how tradeoffs in growth rate at low versus high resource concentrations define an optimum strategy for a single strain [13] or can facilitate coexistence of multiple strains or species when concentrations fluctuate [24, 25]. More recent work has shown how this coexistence can spontaneously evolve if such tradeoffs constrain the effects of mutations [26, 27]. However, the evidence for these tradeoffs, especially on spontaneous mutations, is limited [26–28]. Thus their importance for explaining the evolved variation in growth rate dependence, especially the resource threshold, is unclear.

Here we address this problem using both empirical and modeling approaches. We first collect data for the growth rate dependence on resource concentration across a wide range of organisms and resources, providing the most extensive survey of this data to date. We find that the measured resource thresholds vary over orders of magnitude, even within some single species on the same resource, such as *E. coli* strains on glucose. To better understand the potential causes of this variation, we model evolution for populations under feast-and-famine conditions (batch dynamics with fixed biomass or fixed dilution factor) and steady-state growth (chemostat dynamics). We show how demographic fluctuations, known as genetic drift, inhibit selection on lower thresholds, which leads to a general relationship between the evolved resource threshold, environmental resource concentration, and the effective population size. Using this result, we determine that populations with fixed-bottleneck batch dynamics will evolve resource thresholds that are proportional to the environmental resource concentration, but populations with fixed-dilution batch dynamics evolve thresholds that are practically independent of the environment. Besides providing a testable theory for laboratory evolution experiments, our results help to explain how species evolving under high concentrations can maintain facultative growth at low concentrations and why evolved resource thresholds may not reflect the environment of origin.

RESULTS

The Monod model quantifies growth rate dependence on resource concentration. Consider a population of microbes consuming a resource; we will generally focus on chemical nutrients such as carbon or nitrogen sources, but some aspects of the model apply to other types of resources as well (e.g., prey or light). The best-known dependence of population growth rate g on resource concentration R is the Monod model [7]:

$$g(R) = g^{\max} \cdot \frac{R}{R+K}, \tag{1}$$

where $g^{\max}$ is the maximum growth rate — achieved when the resource is unlimited — and K is a threshold concentration for the resource at which growth rate is slowed to half its maximum (Fig. 1). Decreasing the threshold K therefore allows the population to grow faster at lower resource concentrations. The parameter K is sometimes labeled as the affinity for the resource (see Button [29] for a historical discussion), but this is potentially misleading as K is inversely proportional to ability to grow on the resource. The resource threshold K is also not to be confused with a related but distinct concept of R^* from resource-ratio theory (Methods) [10, 12].

One can derive the Monod model of Eq. (1) by modeling biomass growth as a two-step process, in which uptake of the external resource into the cell occurs at a rate proportional to the external concentration R [30]. However, the dependence of growth rate on resource concentration expressed by Eq. (1) is surprisingly robust to additional model complexities [31, 32], albeit with the resulting traits $g^{\max}$ and K being emergent properties of whole cells or populations. In particular, the threshold K is not necessarily equivalent to the Michaelis-Menten constant for molecular transport [31]. Here we use the Monod model and its parameters as a phenomenological description of microbial growth, as in its original usage [7].

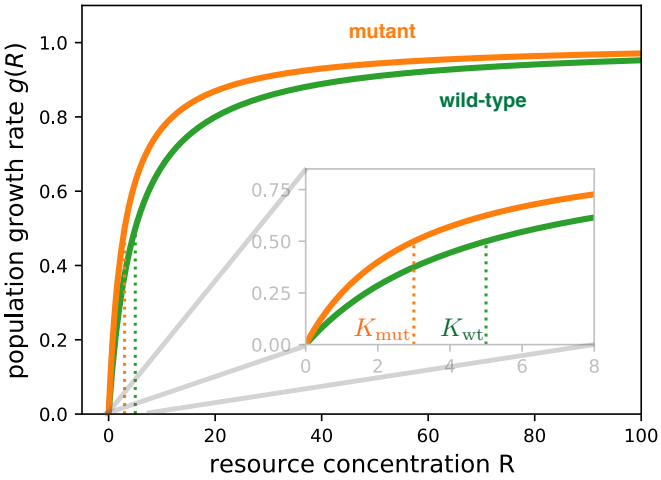

FIG. 1. **Monod model of growth rate dependence on resource concentration.** The population growth rate $g(R)$ as a function of the external resource concentration R for two hypothetical strains: a wild-type (green) and a derived mutant strain (orange), with equal maximum growth rates ($g^{\max} = 1$) but different resource thresholds ($K_{\rm wt} = 5$, $K_{\rm mut} = 3$). The inset shows a magnified view at low concentrations near $K_{\rm wt}$ and $K_{\rm mut}$ (dotted vertical lines). Note that the growth rates do not fully overlap at the highest concentration shown, but eventually converge to the same value $g^{\max}$ outside the range of this plot.

There are several other models of how growth rate depends on resource concentration, such as the linear [33], Blackman [34, 35], Droop [36–39], Bertalanffy [40, 41], Hill (also known as Moser) [42], and Holling [43] models, some of which are equivalent to the Monod model in certain limits (Supplementary Information Sec. S1, compare Table S1). Since some of these models may be more accurate descriptions in certain systems [35, 37–39, 41, 42, 44], we generalize our results to these other models where possible, but focus on the Monod model due to its wider usage and available data.

Resource thresholds vary widely across resources and organisms. To explore the diversity of microbial growth strategies, we have compiled 126 measurements of resource thresholds K from previously-published studies (Methods, Supplementary Data Table 1). This substantially extends previous surveys [45–47] and is the most comprehensive such survey to date to the best of our knowledge. Figure 2A shows an overview of this data, sorted by resource. The data includes a wide range of resources, including sources of carbon, nitrogen, phosphorus, metals, and vitamins. Glucose and silicate have the largest number of measurements, owing to their emphasis in laboratory and marine systems; more recent studies have been especially biased toward glucose (Fig. S1A). Organisms include prokaryotes and eukaryotes as well as autotrophs and heterotrophs (marked by different symbols in Fig. 2A). To guide interpretation of the threshold values, we mark concentrations corresponding to one molecule per cell for typical prokaryotic and eukaryotic cell volumes [48].

Measured values of the threshold K vary over several orders of magnitude, ranging from below 10^{-6} μM (for thiamine and vitamin B12) to above 10^{4} μM (for one glucose measurement). This variation is not attributable to measurement uncertainties, which never exceed 20% in the studies that reported them. It also is not an artifact of technical aspects of the measurements (Fig. S1B) such as temperature (linear regression, $R^2 \approx 4.7 \times 10^{-2}$, $p \approx 3.5 \times 10^{-2}$) or experimental method (linear regression, $R^2 \approx 0.13$, $p \approx 3.5 \times 10^{-2}$).

Instead, most variation of thresholds K corresponds to variation in the identity of the organisms and resources themselves (Fig. S1B). Figure 2B shows a subset of measurements on glucose, which have systematic differences in K between taxa. For example, isolates of *S. cerevisiae* and *Streptococcus* almost all have K values higher than those of *E. coli* (Mann-Whitney U test, $p \approx 2.6 \times 10^{-6}$). Silicate, which also has measurements for many organisms, similarly shows significant variation across species (Fig. S2). Even within some taxa, there is large variation of K; glucose K in *E. coli* varies over three orders of magnitude (Fig. 2B). This variation within a single resource and taxon does not appear to be explained by technical covariates of the measurements (Fig. 2C), but rather corresponds to genetically-distinct strains of *E. coli* (Fig. S3), suggesting that even subspecies-level genetic variation can lead to significant differences in the threshold K. Ferenci [49] reports single target genes, like the membrane-associated lamB or the stress-factor rpoS, that affect the resource threshold of *E. coli* on glucose when mutated. The genetic differences in our dataset are unknown, but we grouped *E. coli* isolates by strain labels to find reproducible glucose thresholds within strains (e.g., ML30, see Fig. S3) despite the large variation within species.

How can we explain this wide variation in resource thresholds? Intuitively, we expect evolution to reduce K, since mutations that reduce K increase growth rate (Eq. (1)). For example, Fig. 1 shows the growth rate dependence for a hypothetical wild-type strain (green line) and a mutant (orange) with lower threshold K. Since this mutant grows faster at all finite resource concentrations, we expect it to be selected over the wild-type. Moreover, this relative advantage may increase at low resource concentrations, which creates stronger selection pressure on populations to reduce their threshold K. This is hinted by some patterns in the data: for example, *E. coli* often grows in mammalian large intestines where there are few simple sugars such as glucose, while *S. cerevisiae* and *Streptococcus* often grow in high-sugar environments (fruit and the oral microbiome, respectively) [50, 51], which could explain their large difference in glucose thresholds.

There is no significant correlation between resource threshold and maximum growth rate. The other trait of the Monod dependence, the maximum growth rate $g^{\max}$, may also play a role in the evolved

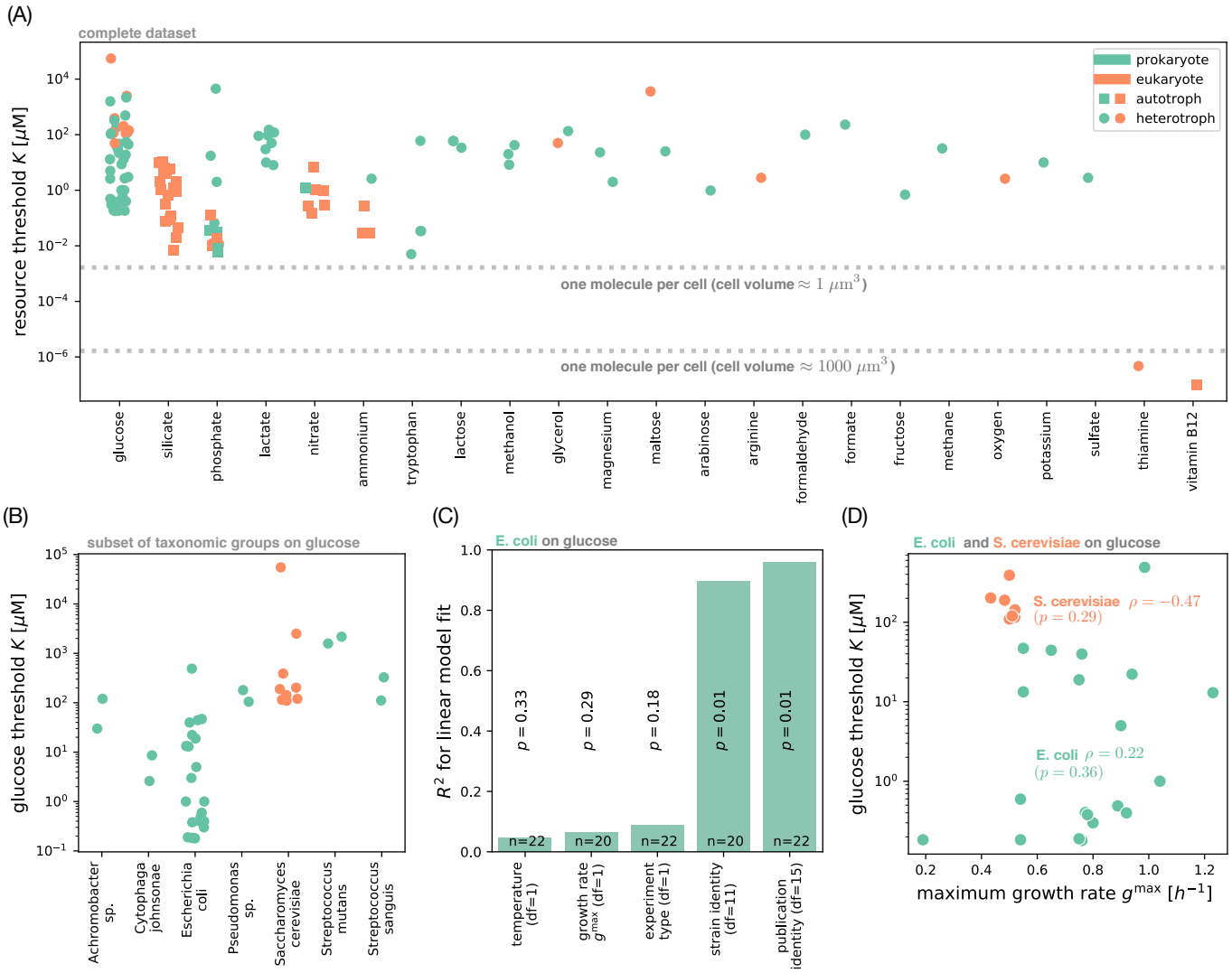

FIG. 2. **Survey of measured resource thresholds K and maximum growth rates $g^{\max}$.** (A) Complete set of resource thresholds K in our survey, grouped by resource (in decreasing order of number of data points). Each point represents a different measurement; color indicates whether the organism is a prokaryote (green) or eukaryote (orange), and shape indicates whether the organism can grow as an autotroph (square) or only as a heterotroph (circle). Dashed lines mark concentrations of one molecule per cell for approximate prokaryotic and eukaryotic cell volumes. (B) Subset of K measurements from panel A for glucose, grouped by taxon (only those with at least two measurements). We use the taxonomic identity given in the original publications, where an ending in *sp.* means the isolate is a representative of the genus but was not identified at the species level. Colors are the same as in panel A. (C) Linear regressions of technical covariates against glucose thresholds $\log_{10} K$ for all *E. coli* measurements, with degrees of freedom (df), number of data points (n), and p-values indicated. (D) Covariation between maximum growth rate $g^{\max}$ and glucose threshold K for isolates of *E. coli* (green) and *S. cerevisiae* (orange), with Spearman rank correlations ρ and p-values. The data shown here is a subset of panel B, since some publications did not report a measurement of maximum growth rate.

variation of K. In particular, many previous studies have considered the possibility of tradeoffs between these traits, such that genotypes growing faster with abundant resources will grow slower when resources are scarce [13, 24–27]. Therefore evolution at high resource concentrations will select more strongly for increasing the maximum growth rate $g^{\max}$ at the expense of the resource threshold K, potentially leading to high values of K. Figure 2D shows the covariation of $g^{\max}$ with K across *E. coli* and *S. cerevisiae* measurements that reported both traits. The *E. coli* data shows a positive correlation indicative of a tradeoff, but it has modest magnitude and low statistical significance (Spearman rank correlation, $\rho \approx 0.22$, $p \approx 0.36$; see also Fig. S4). *Saccharomyces cerevisiae*, on the other hand, shows a weak synergy between the two traits (Spearman rank correlation, $\rho \approx -0.47$, $p \approx 0.29$). Altogether there is no evidence of a significant correlation between K and $g^{\max}$,

suggesting that selection for $g^{\max}$ does not explain the evolved variation in K.

Models of population dynamics with mutations to resource threshold. To more precisely test the factors shaping the evolution of the resource threshold K, especially its dependence on the environmental resource concentration, we turn to a model of population dynamics with mutations altering traits of the Monod growth rate dependence (Methods). We consider a microbial population consisting of a wild-type and a mutant, with biomasses $N_{\rm wt}(t)$ and $N_{\rm mut}(t)$ that vary over time t. They grow at rates depending on the resource concentration R according to the Monod model (Eq. (1)), but with potentially different values of the traits $g^{\max}$ and K depending on the effect of the mutation [24, 27].

We consider three prototypical regimes of population dynamics, which correspond to different relative time scales of biomass growth and resource influx (Methods). In the first case, the population grows as a batch culture with serial transfers; this represents a population where biomass growth is much faster than resource influx. That is, there is a fixed initial concentration R_0 of the resource, and the population grows until the resource is exhausted. Figure 3A shows these dynamics for the hypothetical wild-type and mutant strains of Fig. 1. Although the mutant has the same maximum growth rate $g^{\max}$ as the wild-type, its lower value of K allows it to continue growing fast at lower concentrations of the resource, decelerating more abruptly at the end of growth (see inset of Fig. 3A for more dramatic examples). Then a fixed amount of biomass N_0 is transferred to a new environment with the same initial concentration R_0 of the resource as before, and the cycle repeats (Fig. 3B, top panel). We refer to this regime as *fixed-bottleneck batch dynamics*, since the bottleneck of biomass between transfers is held fixed. In natural environments, these dynamics are plausible for populations that serially colonize new environments [52] or reset to a fixed density by culling [4] between cycles of growth.

The second regime is the same as the first, except instead of transferring a fixed amount of biomass to the next cycle, we transfer a fixed fraction $1/D$, where D is the dilution factor (Fig. 3B, bottom panel); we therefore refer to this regime as *fixed-dilution batch dynamics*. Note that the dilution factor D and the biomass bottleneck N_0 are related according to $D = R_0Y/N_0+1$, where Y is the yield (biomass produced per unit resource; Supplementary Information Sec. S3). These dynamics are plausible for populations that experience a constant death rate between growth cycles or are regularly purged by the environment, as believed to occur in the human gut microbiome [53]. This case is also the most common protocol in laboratory evolution experiments owing to its simplicity [54]. Finally, we consider the regime of *chemostat dynamics*, where the population grows as a continuous culture with a constant supply of the resource and a constant dilution rate d. This represents a population where biomass growth is much slower than resource influx.

Quantifying selection on mutations to resource threshold. The mutant strain will increase or decrease over time under these dynamics. We can quantify selection on the mutant as the rate at which its biomass fraction changes over a time interval Δt (Methods) [55, 56]:

$$s = \frac{1}{\Delta t}\left(\log\left[\frac{N_{\rm mut}(t+\Delta t)}{N_{\rm wt}(t+\Delta t)}\right] - \log\left[\frac{N_{\rm mut}(t)}{N_{\rm wt}(t)}\right]\right). \quad (2)$$

Beneficial mutations will expand at rate $s > 0$, while deleterious mutations will diminish at rate $s < 0$. For batch dynamics, we take the time interval Δt to be the length of a single batch growth cycle, whereas for the continuous dynamics of a chemostat, we use the limit of infinitesimal intervals $\Delta t \to 0$.

We can explicitly calculate how selection according to Eq. (2) depends on the underlying parameters of the model. Let the mutation change the maximum growth rate $g^{\max}$ of the wild-type by a fraction γ and the resource threshold K by a fraction κ:

$$\begin{aligned} g^{\max} \text{ of mutant} &= g^{\max}(1+\gamma), \\ K \text{ of mutant} &= K(1+\kappa). \end{aligned} \quad (3)$$

For batch dynamics, we can show that selection on the mutation per growth cycle is the sum of two components (Methods, Supplementary Information Sec. S4–S6, Fig. S5):

$$s \approx s_{\rm high} + s_{\rm low}, \quad (4a)$$

where

$$s_{\rm high} = \gamma \log\left(1 + \frac{R_0 Y}{N_0}\right), \quad (4b)$$

$$s_{\rm low} = -\kappa\left(\frac{1+\gamma}{1+\kappa+\frac{R_0}{K}+\frac{N_0}{KY}}\right) \cdot \log\left[\left(1+\frac{R_0Y}{N_0}\right)\left(1+\frac{R_0}{K(1+\kappa)}\right)\right]. \quad (4c)$$

The first component, $s_{\rm high}$, measures selection on growth at high resource concentrations, and is therefore proportional to the relative mutational change γ in the trait $g^{\max}$ (Eq. (3)). This mutational effect is weighed by the logarithm of the total fold-change of growth, which equals the dilution factor $D = R_0Y/N_0 + 1$ (Supplementary Information Sec. S3). An important feature of selection $s_{\rm high}$ is that it depends on the nominal maximum growth rate $g^{\max}$, which is always greater than the realized maximum growth rate $g(R_0)$ that actually occurs at the beginning of growth. Therefore the calculation of selection from actual growth data requires an inference of these nominal rates, since the realized rates measured at the

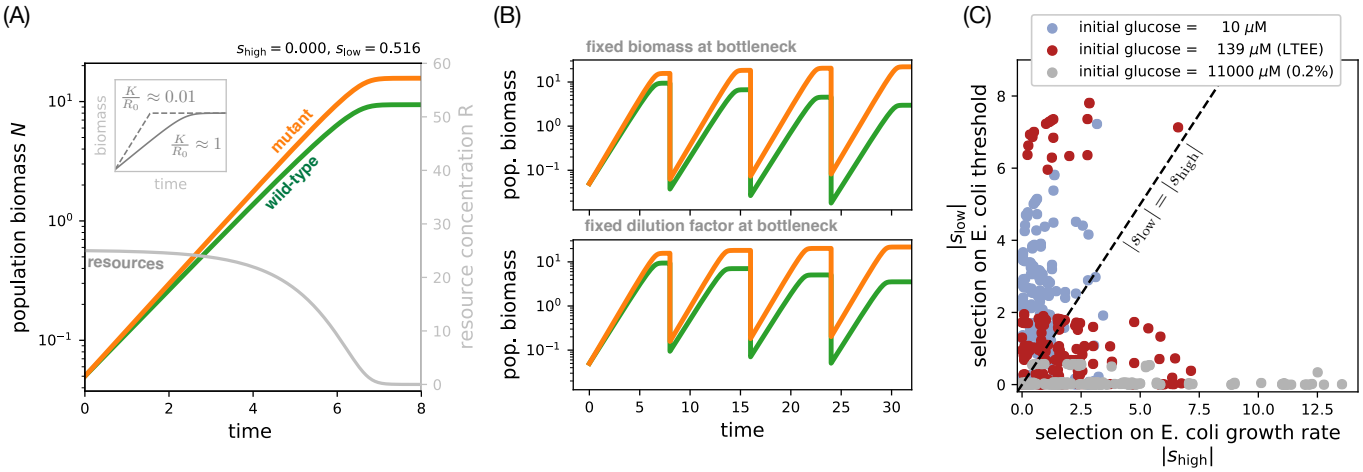

FIG. 3. **Selection on variation in resource thresholds over batch population dynamics.** (A) Simulated growth of wild-type (green) and mutant (orange) strains competing under batch dynamics, with the transient resource concentration (gray) on the right vertical axis (Methods). The strain pair is the same as in Fig. 1; the initial resource concentration is $R_0 = 25$, with strains at equal initial frequencies and equal yields. (B) The same strain competition from panel A continued over multiple growth cycles under fixed-bottleneck batch dynamics (top panel, $N_0 = 0.01$) and fixed-dilution batch dynamics (bottom panel, $D = 100$). (C) Pairwise selection coefficients for experimental isolates of *E. coli* on glucose. Each point is a pair of isolates from Fig. 2D, plotted according to $|s_{\text{high}}|$ and $|s_{\text{low}}|$ with both isolates at equal initial frequencies (Methods). The three colors represent different glucose concentrations. We set the initial cell density to $N_0 = 4.6 \cdot 10^5$ cells/mL and use a separately measured biomass yield of $Y = 3.3 \cdot 10^8$ cells/μmol [22].

beginning of growth curves could produce misleading results if growth begins at low resource concentrations [57].

The second component of selection, s_{low}, corresponds to growth at low resource concentrations, and is proportional to the mutant's relative change κ of the threshold K (Eq. (3)). There is a negative sign in s_{low} since selection is positive for mutations that decrease K ($\kappa < 0$). For the hypothetical mutant and wild-type in Figs. 1 and 3A,B, $s_{\text{high}} = 0$ since the mutant does not change $g^{\max}$, while $s_{\text{low}} \approx 0.516$, since the mutant has a significantly lower threshold K. In the limit of low resource concentrations R_0, the total selection coefficient s becomes proportional to the difference in the ratio $g^{\max}/K$ between mutant and wild-type (Supplementary Information Sec. S6); this ratio (sometimes known as "specific affinity") is a common measure for oligotrophic growth ability [9, 15, 18, 29]. In the Methods and Supplementary Information Sec. S5, we generalize Eq. (4) to arbitrary mutant frequencies and arbitrary dependences (beyond Monod) of growth rate on resource concentration $g(R)$, which extends previous model results [24, 27].

Selection on the mutation under chemostat dynamics is of the same additive form $s \approx s_{\text{high}} + s_{\text{low}}$, except the components are (Supplementary Information Sec. S7)

$$s_{\text{high}} = \gamma d, \tag{5a}$$

$$s_{\text{low}} = -\kappa d \left(\frac{(g^{\max} - d)(1+\gamma)}{(1+\kappa)g^{\max} - \kappa d} \right). \tag{5b}$$

Note that selection under chemostat dynamics is defined per unit time (through the dilution rate d), since the population dynamics are continuous rather than occurring in discrete cycles as in batch cultures.

Selection quantifies variation in growth traits between isolates at different resource concentrations. In Fig. 2 we observed wide variation in resource thresholds K and maximum growth rates $g^{\max}$ across isolates, but the significance of this variation is difficult to assess by itself. For example, glucose K for *E. coli* varied across four orders of magnitude, but how significant is this variation for evolution? Our model of selection gives us precisely the metric to quantify this variation. In Fig. 3C we calculate selection under batch dynamics between all pairs of *E. coli* isolates measured on glucose. Equation (4) shows that selection between strains depends on the resource concentration R_0. While selection on variation in $g^{\max}$ (s_{high}) always increases with higher R_0, selection on variation in K (s_{low}) depends non-monotonically on the concentration R_0, such that selection is maximized at some intermediate concentration (Figs. S6 and S7, Supplementary Information Sec. S8). Intuitively, this optimal concentration approximately equals the threshold K itself.

We therefore calculate selection between *E. coli* isolates at 10 μM glucose, which is in the middle of the range of observed thresholds K, as well as at two higher concentrations corresponding to the conditions of the *E. coli* LTEE (139 μM) [58] and a common laboratory concentration (11000 μM $\approx$ 0.2% w/v). Figure 3C indeed shows that variation in the thresholds K is highly significant for evolution at concentrations around the threshold values, whereas at the highest concentration, selection on the variation in K is small compared to the selection in

$g^{\max}$.

The resource threshold evolves downward over successive mutations. With our model of population dynamics, we can predict how the traits of the Monod growth rate dependence (Eq. (1)) will evolve over long times. For simplicity, we focus on the "strong-selection weak-mutation" (SSWM) regime of evolutionary dynamics, where each new mutation either fixes or goes extinct before the next mutation arises (Methods, Fig. S8) [59]. In the Discussion we address generalizations of our results to populations where many mutations simultaneously compete (clonal interference) [60].

We first simulate a population growing under fixed-bottleneck batch dynamics, with an initial threshold K that is higher than the external resource concentration R_0; the population therefore decelerates gradually into starvation over each growth cycle (Fig. 4A, left inset). Mutations then regularly arise and alter the threshold K with a random effect size κ (Eq. (3), Methods). Each mutation stochastically fixes or goes extinct according to a fixation probability, which depends on the mutation's selection coefficient (Eq. (4), Methods). Over time these beneficial mutations accumulate and the threshold K systematically decreases. By the end of the simulation, the threshold K is 1000 times smaller than the resource concentration R_0, leading to growth curves that grow much faster and abruptly decelerate into starvation (Fig. 4A, right inset).

Such an abrupt arrest is, for example, realized by *E. coli* in glucose-limited batch culture through a dynamic surge in gene expression late in the growth cycle [61], often involving the use of separate transporters with lower Michaelis-Menten constants [62]. The presence of these transporter systems has been raised as evidence for substantial evolution of the species at micromolar glucose concentrations [8, 62, 63]. But from our model, a feast-and-famine environment dominated by concentrations orders of magnitude higher would still allow *E. coli* to evolve the low resource threshold K and underlying molecular machinery found today.

Adaptation in the resource threshold stalls when it reaches selection-drift balance. The threshold K does not evolve downward forever; in Fig. 4A adaptation slows down and the threshold levels off after a few tens of thousands of mutations, even though there is no change in the supply of beneficial mutations. This occurs because selection on beneficial mutations is inhibited by random demographic fluctuations in the population, known as genetic drift [64]. The strength of genetic drift is measured by $1/N_{\mathrm{e}}$, where N_{e} is the effective population size [65]; smaller populations experience greater fluctuations. In the simplest cases, N_{e} is proportional to the actual ("census") population size, but in more complex systems N_{e} may depend on other aspects of demography (such as spatial dynamics [66] or age structure [67]) as well as additional sources of noise in the population dynamics [68].

Beneficial mutations will therefore no longer fix with high probability if their selection equals genetic drift, a condition known as selection-drift balance [69–71]:

$$s = \frac{1}{N_{\mathrm{e}}}. \tag{6}$$

Note that N_{e} here specifically refers to the effective population size for the fixation probability of a neutral mutation ($1/N_{\mathrm{e}}$; Supplementary Information Sec. S9), since there are different concepts of effective population size for different phenomena [72]. Selection-drift balance occurs in our model under batch dynamics because the growth deceleration phase becomes shorter as K decreases over evolution (insets of Figs. 3A and 4A), which means there is weaker selection to reduce it further. Once the threshold K becomes sufficiently small, selection is no longer strong enough to overcome genetic drift (Supplementary Information Sec. S9, Fig. S9).

By combining Eqs. (4) and (6), we can calculate the value of the evolved threshold at which selection-drift balance occurs (Supplementary Information Sec. S10, Fig. S10). Under typical limits of the parameters, the evolved threshold is approximately (Supplementary Information Sec. S10)

$$K_{\mathrm{evo}} \approx \frac{R_0}{N_{\mathrm{e}}|\kappa_{\max}| \log(N_{\mathrm{e}}|\kappa_{\max}|R_0 Y/N_0)}, \tag{7}$$

where $\kappa_{\max}$ is the maximum effect size of a beneficial mutation reducing K. We calculate an example of K_{evo} (using an exact numerical solution to Eqs. (4) and (6)) in Fig. 4A (dashed green line), which corresponds well with the simulations. This result is robust to a wide range of effective population sizes and frequency-dependent effects (Fig. S11, Methods).

One salient feature of Eq. (7) is that the evolved threshold K_{evo} scales inversely with the effective population size N_{e}, as shown in Fig. 4B. That is, larger populations or those with lower genetic drift can evolve proportionally lower thresholds K_{evo} that are orders of magnitude lower than the environmental resource concentration R_0. This suggests why we observe such low thresholds K for many organisms and resources (Fig. 2); this also explains why these thresholds are difficult to measure from time-series data, since low thresholds produce extremely abrupt deceleration at the end of growth (insets of Figs. 3A and 4A and Fig. S12; Supplementary Information Sec. S11). Hints of the influence of N_{e} are found in ammonia-oxidizing archaea and bacteria from marine environments, which tend to have lower resource thresholds than lineages isolated from soil [17]. Assuming that these measurements more or less reflect cell growth rate, our scaling relationship Eq. (7) suggests that this ordering can arise from the smaller effective population size N_{e} for spatially-structured environments like soil.

The other important feature of Eq. 7 is the dependence of the evolved threshold K_{evo} on the resource concentration R_0. For fixed effective population size N_{e}, there is an

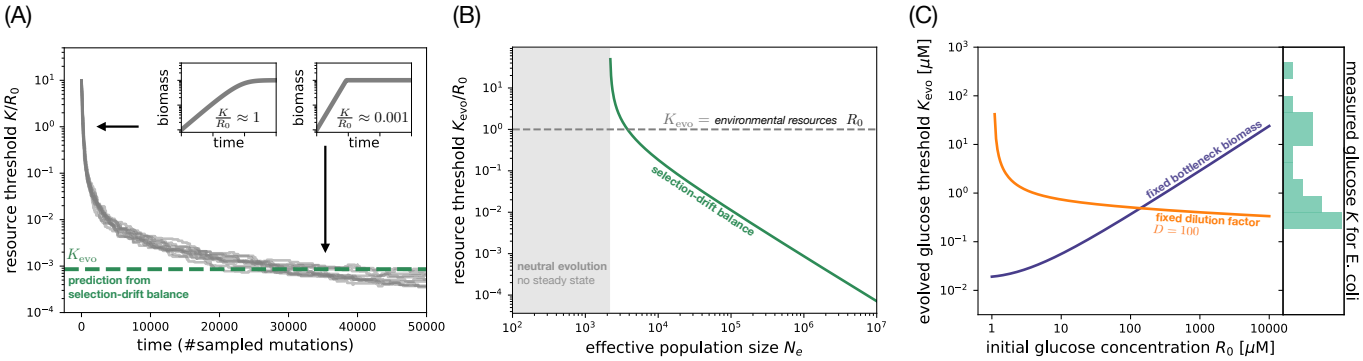

FIG. 4. **Evolution of the resource threshold.** (A) The resource threshold K evolving under fixed-bottleneck batch dynamics (Methods). Each gray line is one of 10 independent stochastic simulations using an effective population size $N_e = 1000$ and mutation effects κ drawn from a uniform distribution (Methods). The insets show the growth curve in a single batch cycle before adaptation (left inset) and at the final state (right inset). The green dashed line marks our prediction K_{evo} at selection-drift balance. (B) Evolved resource threshold K_{evo} as a function of the effective population size N_e. In the gray region, the effective population size is too small and all evolution is neutral. If N_e is sufficiently large (white region), the evolved resource threshold K_{evo} has selection-drift balance along the green line. Parameters are $|\kappa_{max}| = 0.001$, $g^{max} = 1$, $N_0 = 0.01$, and $Y = 1$ for both strains. (C) The evolved glucose threshold K_{evo} as a function of initial glucose concentration R_0 for two regimes of batch dynamics: fixed-bottleneck dynamics (blue line) or fixed-dilution dynamics (orange line). We use parameters based on the LTEE: $N_0 = 4.6 \cdot 10^5$ cells/mL (for fixed-bottleneck case), $D = 100$ (for fixed-dilution case), $N_e = V \cdot N_0$ where $V = 10$ mL, $g^{max} = 0.888$/h, and $Y = 3.3 \cdot 10^8$ cells/μmol [22]. We also set $\kappa_{max} = 6 \cdot 10^{-6}$ (Fig. S15). On the right axis is a histogram of glucose threshold K data for *E. coli* isolates (from Fig. 2B). In all panels we calculate K_{evo} from a numerical solution of Eqs. (4) and (6).

optimal value of R_0 that minimizes the evolved threshold K_{evo} (left insets of Fig. S10A,B), just as we observed for selection on individual mutations (Fig. S6). We note that for sufficiently low values of the effective population size N_e, genetic drift is stronger than selection on any mutation κ (Fig. S9), and so there the threshold K evolves neutrally (gray region in Fig. 4B).

In contrast to batch dynamics, selection under chemostat dynamics does not depend on the threshold K itself (Eq. (5)). Intuitively, this is because reductions in K cause the environmental resource concentration to decrease proportionally (Methods), such that the growth rate remains constant. Not only does this keep a constant strength of selection on new mutations, but the effective population size will actually increase as K evolves lower (Methods), making beneficial mutations even easier to fix. Therefore selection-drift balance never occurs for K under chemostat dynamics; the threshold K will continue to evolve lower until adaptation is limited by the supply of mutations or other factors (Discussion). Note that selection-drift balance also does not occur for mutations to the maximum growth rate g^{max} under either batch or chemostat dynamics, since selection does not depend on the magnitude of growth rate (Eqs. (4) and (5)).

Population dynamics can decouple the evolved threshold from the resource concentration. In general the effective population size N_e that controls genetic drift may be shaped by a variety of demographic factors besides the census population size [65]. However, in well-mixed batch cultures, N_e is primarily determined by the number of cells at the bottleneck of each transfer [69, 73]; we assume that other sources of stochasticity (such as individual cell division events) are much smaller than the sampling noise of these transfers. Therefore the effective population size N_e is proportional to the bottleneck biomass N_0 (assuming constant biomass per cell).

Under fixed-bottleneck batch dynamics, the effective population size N_e is thus an independent parameter of the population, so that the strength of genetic drift does not depend on the resource concentration (Fig. S13). In this case, the threshold K_{evo} evolves in approximately linear proportion to the resource concentration R_0 (Eq. (7), Figs. 4C and S14A), making the evolved threshold a biomarker of the resource's environmental concentration. This is consistent with our original speculation about the systematic differences in glucose K between *E. coli* and *S. cerevisiae*, owing to the different glucose availability in their different environments.

However, for fixed-dilution batch dynamics, the bottleneck biomass N_0, and therefore the effective population size, are coupled to the resource concentration R_0 because the dilution factor D is fixed: $N_e \propto N_0 = R_0 Y/(D-1)$ (Methods). This is because increasing the resource concentration increases the biomass at the end of each growth cycle, but then the bottleneck biomass must also increase proportionally to hold the dilution factor fixed. The scaling of N_e with R_0, though, cancels out the scaling of K_{evo} with R_0 in Eq. (7), leading to an evolved threshold K_{evo} that is approximately independent of the environmental concentration R_0 (Figs. 4C and S14B). Conceptually, this occurs because increasing the resource R_0 decreases selection on the mutation but also decreases genetic drift, since the effective population size N_e increases (Fig. S13). Thus, the population

dynamics decouple the evolved threshold from the environmental concentration.

This has drastic consequences for interpreting empirical variation. We predict the evolved threshold K_{evo} for *E. coli* on glucose as a function of glucose concentration R_0 in Fig. 4C, using parameters estimated from the LTEE (Fig. S15). On the same plot, we show a histogram of all measured glucose thresholds for *E. coli* (from Fig. 2B) on the right vertical axis. We see that, under fixed-bottleneck batch dynamics, we would expect *E. coli* to have evolved in glucose concentrations above 100 μM to account for the observed glucose thresholds. However, under fixed-dilution batch dynamics, the evolved glucose threshold depends so weakly on the environmental concentration that almost any concentration of glucose is possible to explain the data.

DISCUSSION

Modeling insights to interpret threshold data. Isolates in our survey of data vary widely in their evolved resource thresholds (Fig. 2A); even isolates of *E. coli* on glucose span four orders or magnitude (Fig. 2B). Our model results now provide an evolutionary framework for interpreting this variation. In particular, the model suggests that we should not be surprised by this wide variation, given the several factors — and not just environmental concentration of a resource — that determine the evolved resource threshold. Furthermore, the model makes several testable predictions that we can validate using laboratory evolution experiments. For example, by evolving populations at different resource concentrations and under different batch protocols, one can directly test our predictions that adaptation will be fastest at resource concentrations near K under fixed bottleneck batch dynamics (Fig. S6), but fastest at the lowest resource concentrations under fixed-dilution dynamics (Fig. S7).

To make similar predictions for natural environments, we would need to know additional parameters such as resource concentrations and details of the population dynamics. Given that these parameters are often difficult to measure, the inverse problem may be more valuable: can we use the evolved threshold K as a biomarker to infer environmental conditions or population dynamics? This logic is often implicit in environmental studies, which attempt to draw conclusions about the environmental conditions of an isolate based on its abilities to grow at different resource concentrations [15–18]. However, our model shows that it is not as simple as assuming the threshold K for a resource is proportional to its concentration in the environment, since that proportionality is altered by the population dynamics, at least through the effective population size N_{e} (Eq. (7)). In particular, this proportionality is confounded in the case of fixed-dilution batch dynamics, where the evolved threshold K is largely independent of the resource concentration R_0 (Fig. 4C). Under fixed-bottleneck batch dynamics, though, the linear scaling of K and R_0 does approximately hold. In this case, one can compare two populations with unknown, but identical effective population sizes N_{e} and mutation effects κ; for example, two isogenic populations located at different points along a resource gradient. In this case, one can calculate the ratio of evolved resource thresholds K_{evo} for the two populations to estimate the ratio of resource concentrations. But in many scenarios, one might not even know the type of bottlenecks the population is experiencing. To classify the population dynamics as fixed-bottleneck or fixed-dilution, one could correlate a set of evolved thresholds K_{evo} with their different resource concentrations R_0; a strong linear correlation would support fixed-bottleneck batch dynamics, while little to no correlation would indicate fixed-dilution batch or chemostat dynamics.

Role of the mutation supply in shaping evolved resource thresholds. We have focused on the role of selection-drift balance as a null model for the evolved variation in resource thresholds, since the competition between selection and genetic drift is a universal feature of all evolving populations. In doing so we have assumed the supply of mutations on K is constant, but real populations will at some point run out of beneficial mutations on the threshold K, potentially reaching this mutation-selection balance before selection-drift balance [70]. In particular, this may be the main constraint on K in chemostat conditions, where we have shown there is no selection-drift balance. But besides limitations in their supply, many mutations will also be pleiotropic, affecting both the resource threshold K and the maximum growth rate $g^{\max}$ (as well as possibly other traits) simultaneously. The correlation between pleiotropic effects on both traits is important: if pleiotropy is synergistic, so that mutations that decrease K also tend to increase $g^{\max}$, then population might evolve lower K than otherwise expected since its selection is enhanced by additional selection on $g^{\max}$. On other other hand, if there is a tradeoff between K and $g^{\max}$, the population might evolve higher K if its selection is outweighed by selection for higher $g^{\max}$. Indeed, this is what appears to happen in the LTEE, where K for glucose actually increased over the first 2000 generations, but that was offset by a stronger improvement in the maximum growth rate $g^{\max}$ [22].

Such a tradeoff between K and $g^{\max}$ is interesting from an evolutionary point of view, since the population can then diversify into stably coexisting lineages. While there is significant theoretical work on this hypothesis [24–27], it has limited empirical evidence. Elbing et al. [74] found a tradeoff between Michaelis-Menten parameters K_{M} and $V_{\max}$ for a set of yeast strains with engineered transporter proteins. However, this tradeoff is observed at the level of nutrient uptake and does not necessarily correspond to a tradeoff in the population growth traits; Snoep et al. [31] showed the glucose threshold K could vary more than twofold from the corresponding threshold K_{M} for nutrient uptake, a possibility that has also been shown by mechanistic models [32]. Wirtz [28] presents a tradeoff

between population growth traits K and $g^{\max}$ for *E. coli* on glucose, but it is based on few data points ($n = 12$) and mostly from measurements of nutrient uptake that are insufficiently documented (some trait estimates could not be reproduced given the references). In the larger set of data we have collected in this work (Fig. 2D), we find no compelling evidence of a correlation; *E. coli* shows a weak but insignificant tradeoff, while *S. cerevisiae* shows a slight synergy [44].

Interpretation of this tradeoff (or the lack thereof) is also complicated by the sample of strains and environmental conditions being considered. For the tradeoff to affect the evolved threshold as we have discussed, the tradeoff must exist across the spectrum of spontaneous mutations available to an organism (i.e., there is an underlying physiological constraint). This has also been the underlying assumption of previous models on this topic [24–27]. Testing this would require a distribution of K and $g^{\max}$ measurements over a large mutant library in a single environment, which to our knowledge has not been done. However, even in the absence of an underlying correlation in mutation effects, such a tradeoff could still emerge across clones within a rapidly evolving population, at least transiently [75, 76]. Experiments with soil bacteria, designed by Velicer et al. [77] to evolve a tradeoff in acid degradation, found that lineages adapting for 500 generations in a low concentration environment also become superior competitors in high concentrations and vice versa. This study, though, does not identify underlying changes in maximum growth rate $g^{\max}$ and resource threshold K. Further systematic measurements of these traits within and between populations will be necessary to resolve the issue of a tradeoff in the future.

Other factors shaping evolved resource thresholds. Besides mutation supply, there are other phenomena that may lead to different evolved outcomes for the threshold K. One important assumption in our model is that we only consider a single resource, whereas real populations are dependent on several resources [78]. Many of these resources may be rarely or never limiting, and therefore their thresholds K will evolve only as byproducts of selection on mutations for other traits. In this sense many observed resource thresholds may actually be spandrels, an evolutionary term (defined in analogy with the architectural structure) for traits that evolve for reasons other than direct selection [79].

We can predict the consequences of relaxing other assumptions in our model as well. For example, simultaneous competition of multiple mutations (clonal interference) generally reduces the efficacy of selection [80, 81], which would make it more likely to evolve higher thresholds than what we predict from SSWM dynamics. Another assumption in our model is that the population under batch dynamics always grows until complete exhaustion of the resources during each cycle, but earlier transfers could reduce the amount of growth occurring during deceleration, which would reduce selection on the threshold K. However, the population may adapt its maximum growth rate to simply saturate earlier and restore selection on its deceleration phase. Finally, populations may simply not have had enough time to reach selection-drift balance, since this will typically take a timescale of the order N_{e} generations (Fig. S11) [82].

Population dynamics are essential for understanding microbial ecology. Broadly speaking, our results provide a valuable example of how ecological traits are influenced by factors other than abiotic environmental features. In particular, we have shown how population dynamics can confound our naive expectations for the evolutionary fate of such traits. While here we have focused on the role of genetic drift, other potentially important factors include mutation supply, pleiotropy, recombination, and spatial structure. Altogether our results mean that the threshold K may not be a reliable biomarker of environmental resource concentrations. This does not mean that K evolves independently of the environment, however. Rather, it is linked to additional environmental processes like the bottleneck between growth cycles. To understand the systematic differences between species, we need to know not only the resource concentrations they have evolved in, but also which type of population dynamics best reflects the time scales of growth, death, and resource supply in natural environments.

METHODS

Literature survey of measured growth rate dependence on resources. We collected measurements of Monod model parameters (K and $g^{\max}$; Eq. (1)) through a targeted literature search that included prior surveys and reviews as well as original research papers. We included only experiments that directly measured population growth rates, rather than nutrient uptake rates. In all but two cases, we traced data from surveys and reviews back to their original papers, which we report in Supplementary Data Table 1. If the original K value was reported as weight per volume, we converted these into units of micromolar (μM) using the calculated molecular weight of the compound's chemical formula. We preserved significant digits from the original study. See Supplementary Data Table 1 for more details.

Model of population dynamics in a batch culture. The dynamics of the wild-type and mutant biomasses $N_{\mathrm{wt}}(t)$ and $N_{\mathrm{mut}}(t)$ and the extracellular resource concentration $R(t)$ are given by the following differential equations [24, 27]:

$$\begin{aligned} \frac{1}{N_{\mathrm{wt}}}\frac{dN_{\mathrm{wt}}}{dt} &= g_{\mathrm{wt}}(R), \qquad N_{\mathrm{wt}}(0) = (1-x)\cdot N_0, \\ \frac{1}{N_{\mathrm{mut}}}\frac{dN_{\mathrm{mut}}}{dt} &= g_{\mathrm{mut}}(R), \quad N_{\mathrm{mut}}(0) = x\cdot N_0, \\ \frac{dR}{dt} &= -\frac{1}{Y_{\mathrm{wt}}}\frac{dN_{\mathrm{wt}}}{dt} - \frac{1}{Y_{\mathrm{mut}}}\frac{dN_{\mathrm{mut}}}{dt}, \qquad R(0) = R_0. \end{aligned} \tag{8}$$

See Table S2 for a summary of the main notation and definitions used throughout this article. Growth begins with an external resource concentration R_0 and total biomass N_0, a fraction x of which is the mutant strain. The strains then grow exponentially with rates $g_{\mathrm{wt}}(R)$ and $g_{\mathrm{mut}}(R)$, which depend on the extracellular resource concentration $R(t)$; here we neglect other growth dynamics such as lag [56, 83] and death [84] for simplicity, but they are

straightforward to add within this framework. The resource concentration $R(t)$ declines in proportion to growth of biomass, where the yields $Y_{\rm mut}$ and $Y_{\rm wt}$ for each strain set the amount of new biomass per unit resource. Here we neglect resource consumption due to maintenance of existing biomass [85], since we expect maintenance consumption to be much less than growth consumption during rapid growth. Growth continues until the resource is depleted or the growth rates reach zero. While it is difficult to analytically solve these dynamics in general, it is straightforward to numerically solve the model for a given set of parameters (Supplementary Information Sec. S2).

Once the resource R is depleted, we transfer a fraction $1/D$ of the population to an environment with a new supply of resources at the original concentration R_0, after which the population resumes growth in the new environment according to Eq. (8). The factor D is known as the dilution factor and is the ratio of the total biomass at the end of the previous growth cycle ($R_0\bar{Y} + N_0$, where $\bar{Y}$ is the effective population yield; see Table S2 and Supplementary Information Sec. S3) and the total biomass at the beginning of the next growth cycle (N_0) [76]:

$$D = \frac{R_0\bar{Y}}{N_0} + 1. \tag{9}$$

This constraint establishes the two possible protocols of serial transfers: either fixing the biomass bottleneck size N_0 (Fig. 3B, top panel) or fixing the dilution factor D (Fig. 3B, bottom panel), with the other quantity being determined by Eq. 9.

Model of populations in continuous culture. Similar to the batch model of Eq. (8), the dynamics of biomass and resource concentration under continuous culture are

$$\begin{aligned}
\frac{1}{N_{\rm wt}}\frac{dN_{\rm wt}}{dt} &= g_{\rm wt}(R) - d, \qquad N_{\rm wt}(0) = (1-x)\cdot N_0,\\
\frac{1}{N_{\rm mut}}\frac{dN_{\rm mut}}{dt} &= g_{\rm mut}(R) - d, \qquad N_{\rm mut}(0) = x\cdot N_0,\\
\frac{dR}{dt} &= -g_{\rm wt}(R)\frac{N_{\rm wt}(t)}{Y_{\rm wt}} - g_{\rm mut}(R)\frac{N_{\rm mut}(t)}{Y_{\rm mut}} + d(R_{\rm source} - R(t)),\\
&\qquad R(0) = R_0.
\end{aligned} \tag{10}$$

where $R_{\rm source}$ is the concentration of the resource in the source media fed into the culture. In a laboratory chemostat, the dilution rate $d = \omega/V$, where ω is the outflow rate (volume per time) and V is the volume of the culture vessel [3]. In the SSWM regime where mutations arise only rarely, we can assume that the mutant arises on the background of the wild-type at steady state growth. Let $N^*_{\rm wt}$ be the steady-state concentration of wild-type biomass and R^* be the steady-state concentration of the resource. Note that R^* here is the chemostat-specific realization of the ecological concept of a minimum resource concentration required for positive net growth, as used in resource-ratio theory [10, 12]. Since $dN_{\rm wt}/dt = 0$ in steady state, the resource concentration R^* must satisfy $g_{\rm wt}(R^*) = d$. For the Monod model, this means $R^* = K_{\rm wt}d/(g^{\rm max}_{\rm wt} - d)$. Note that this concentration R^* is independent of the source concentration $R_{\rm source}$. Using the steady-state condition for the resource $dR/dt = 0$, we can then obtain the steady-state biomass concentration $N^*_{\rm wt} = (R_{\rm source} - R^*)Y_{\rm wt}$.

This establishes a feasability condition for steady state: the dilution rate d must be less than the growth rate at the source concentration $g_{\rm wt}(R_{\rm source})$. This criterion has been used by Jannasch [5, 46] to define a *minimum resource threshold* required for population growth at a given dilution factor d. This minimum resource threshold corresponds to the steady-state concentration R^*, which is related to the parameter K but also depends on d.

Selection coefficient for mutations. For a general growth rate dependence $g(R)$, the selection coefficient for a mutant per batch growth cycle is (Supplementary Information Sec. S5)

$$s \approx \int_0^{R_0} \left(\frac{g_{\rm mut}(R) - g_{\rm wt}(R)}{\bar{g}(R)}\right)\left(\frac{1}{R_0 + \frac{N_0}{\bar{Y}} - R}\right) {\rm d}R, \tag{11}$$

where $\bar{g}(R)$ is the effective population growth rate (Table S2). This approximation holds as long as selection on the mutation is not too strong, meaning that its frequency does not change too much during a single growth cycle (Fig. S16; see Supplementary Information Sec. S5 for a complete derivation). Equation (4) is a special case of Eq. 11 where $g(R)$ is given by the Monod model (Eq. (1)) and the mutant is at infinitesimal frequency. While in the main text we focus on variation only in K, Eqs. (4) and (11) are also valid for strains with variation in both K and $g^{\rm max}$, such as case of a "gleaner-opportunist" tradeoff (Fig. S17) [12, 24, 27, 32].

Equation (11) shows that total selection over the growth cycle integrates the relative difference in growth rate between the mutant and wild-type at each resource concentration R (left factor of the integrand), ranging from the initial concentration $R = R_0$ to its final value $R = 0$ when growth stops. Because this difference is only relative to the average of the growth rates $\bar{g}(R)$, it means that selection only depends on the ratio of the growth rates $g_{\rm wt}(R)/g_{\rm mut}(R)$ at each concentration of the resource R. Therefore we can get the same selection on mutants even for vastly different growth rate resource dependences as long as the ratio is the same. These relative growth rate differences are weighted by the second factor in the integrand, which is larger for resource concentrations near the initial concentration $R = R_0$ and smaller for low concentrations (Fig. S18). Therefore growth rate differences at the beginning of growth make larger contributions to selection than growth rate differences at the end of growth (Supplementary Information Sec. S8, Fig. S18).

The selection coefficient per unit time for the chemostat case is (Supplementary Information Sec. S7)

$$s \approx s_{\rm high} + s_{\rm low}, \tag{12a}$$

where

$$s_{\rm high} = \frac{g^{\rm max}_{\rm mut} - g^{\rm max}_{\rm wt}}{\bar{g}^{\rm max}}\bar{g}(R), \tag{12b}$$

$$s_{\rm low} = -\left(\frac{K_{\rm mut} - K_{\rm wt}}{R + Z}\right)\left(\frac{g^{\rm max}_{\rm wt} g^{\rm max}_{\rm mut}}{(\bar{g}^{\rm max})^2}\right)\bar{g}(R), \tag{12c}$$

where $\bar{g}(R)$ is the mean population growth rate at resource concentration R (Supplementary Information Sec. S5). We obtain Eq. (5) as a special case of Eq. (12) by taking the mutant to be at infinitesimal frequency and the wild-type to be under steady-state growth (with resource concentration R^* and biomass $N^*_{\rm wt}$ as defined above).

Evolutionary simulations. We simulate evolutionary trajectories by first randomly sampling a mutation effect κ from a uniform distribution on $[-0.1, 0.1]$. We then calculate the selection coefficient of this mutation using Eq. (4), and the fixation probability according to [86]

$$p(s) = \frac{1 - e^{-2s}}{1 - e^{-2N_{\rm e}s}}, \tag{13}$$

where $N_{\rm e}$ is the effective population size. We then randomly accept or reject the mutation according to this probably, and then the cycle repeats with a new mutation (Fig. S8). We consider frequency-dependence of selection (Supplementary Information Sec. S9), but Fig. S11D-F shows that populations evolve to the same resource threshold. We also repeat our selection-drift balance analysis for mutations that appear within the growth cycle, but we conclude that this does not change the evolved resource threshold $K_{\rm evo}$ (Supplementary Information Sec. S9).

ACKNOWLEDGMENTS

JWF and MM were supported by an Ambizione grant from the Swiss National Science Foundation (PZ00P3_180147). NAH was supported by the Principles of Microbial Ecosystems collaboration of the Simons Foundation (grant ID 542379) and an ETH Zurich Career Seed Grant (SEED-26 21-2). We thank Ayush Pathak for a critical reading of the manuscript.

[1] M. Schaechter, J. L. Ingraham, and F. C. Neidhardt. *Microbe*. ASM Press, Washington, DC, 2006.

[2] T. E. Shehata and A. G. Marr. Effect of nutrient concentration on the growth of escherichia coli. *Journal of Bacteriology*, 107:210–216, 1971.

[3] Nicolai S. Panikov. *Microbial Growth Kinetics*. London: Chapman & Hall, 1995.

[4] David L. Kirchman. Growth rates of microbes in the oceans. *Annual Review of Marine Science*, 8:285–309, 2016.

[5] Jeanne S. Pointdexer. Oligotropy, in. *Advances in Microbial Ecology*, pages 63–89, 1981.

[6] Noah Fierer, Mark A. Bradford, and Robert B. Jackson. Toward an ecological classification of soil bacteria. *Ecology*, 88:1354–1364, 2007.

[7] J. Monod. The growth of bacterial cultures. *Annu Rev Microbiol*, 3:371–394, 1949.

[8] Arthur L. Koch. The adaptive responses of escherichia coli to a feast and famine existence. *Advances in Microbial Physiology*, 6:147–217, 1971.

[9] Don K. Button. Kinetics of nutrient-limited transport and microbial growth. *Microbiological Reviews*, 49:270–279, 1985.

[10] D. Tilman. *Resource competition and community structure*. Princeton University Press, Princeton, NJ, 1982.

[11] T. E. Miller, J. H. Burns, P. Munguia, E. L. Walters, J. M. Kneitel, P. M. Richards, N. Mouquet, and H. L. Buckley. A critical review of twenty years' use of the resource-ratio theory. *Am Nat*, 165:439–448, 2005.

[12] Joey R. Bernhardt, Pavel Kratina, Aaron Louis Pereira, Manu Tamminen, Mridul K. Thomas, and Anita Narwani. The evolution of competitive ability for essential resources. *Philosophical Transactions of the Royal Society B: Biological Sciences*, 375(1798):20190247, May 2020. Publisher: Royal Society.

[13] James P. Grover. *Resource Competition*. Springer US, 1997.

[14] Erik Askov Mousing, Katherine Richardson, and Marianne Ellegaard. Global patterns in phytoplankton biomass and community size structure in relation to macronutrients in the open ocean. *Limnology and Oceanography*, 63:1298–1312, 2018.

[15] Willm Martens-Habbena, Paul M. Berube, Hidetoshi Urakawa, José R. de la Torre, and David A. Stahl. Ammonia oxidation kinetics determine niche separation of nitrifying archaea and bacteria. *Nature*, 461:976–979, 2009.

[16] James I. Prosser and Nicol W. Graeme. Archaeal and bacterial ammonia-oxidisers in soil: The quest for niche specialisation and differentiation. *Trends in Microbiology*, 20:523–31, 2021.

[17] Dimitri K. Kits, Christopher J. Sedlacek, and Elena V. Lebedeva et al. Kinetic analysis of a complete nitrifier reveals an oligotrophic lifestyle. *Nature*, 549:269–272, 2017.

[18] Man-Young Jung, Christopher J. Sedlacek, K. Dimitri Kits, Anna J. Mueller, Sung-Keun Rhee, Linda Hink, Graeme W. Nicol, and et al. Ammonia-oxidizing archaea possess a wide range of cellular ammonia affinities. *The ISME Journal*, 16:272–283, 2022.

[19] Daniel Dykhuizen and Daniel Hartl. Evolution of competitive ability in escherichia coli. *Evolution*, 35:581, 1981.

[20] Karin Kovárŏvá. Growth kinetics of escherichia coli: Effect of temperature, mixed substrate utilization and adaptation to carbon-limited growth. *Ph.D. thesis, ETH Zurich*, 1996.

[21] Julian Adams, Charlotte Paquin, Paul W. Oeller, and Lester W. Lee. Physiological characterization of adaptive clones in evolving populations of the yeast, saccharomyces cerevisiae. *Genetics*, 110:173–185, 1985.

[22] Farida Vasi, Michael Travisano, and Richard E. Lenski. Long-Term Experimental Evolution in Escherichia coli. II. Changes in Life-History Traits During Adaptation to a Seasonal Environment. *The American Naturalist*, 144(3):432–456, September 1994.

[23] Samuel Frederick Mock Hart, Chi-Chun Chen, and Wenying Shou. Pleiotropic mutations can rapidly evolve to directly benefit self and cooperative partner despite unfavorable conditions. *eLife*, 10:e57838, January 2021. Publisher: eLife Sciences Publications, Ltd.

[24] Frank M. Stewart and Bruce R. Levin. Partitioning of Resources and the Outcome of Interspecific Competition: A Model and Some General Considerations. *The American Naturalist*, 107(954):171–198, March 1973. Publisher: The University of Chicago Press.

[25] Antony M Dean. Protecting Haploid Polymorphisms in Temporally Variable Environments. *Genetics*, 169(2):1147–1156, February 2005.

[26] Robert E. Beardmore, Ivana Gudelj, David A. Lipson, and Laurence D. Hurst. Metabolic trade-offs and the maintenance of the fittest and the flattest. *Nature*, 472(7343):342–346, April 2011. Bandiera_abtest: a Cg_type: Nature Research Journals Number: 7343 Primary_atype: Research Publisher: Nature Publishing Group Subject_term: Evolutionary theory;Microbial ecology;Mutation Subject_term_id: evolutionary-theory;microbial-ecology;mutation.

[27] Meike T. Wortel. Evolutionary coexistence in a fluctuating environment by specialization on resource level. Technical report, September 2021. Company: Cold Spring Harbor Laboratory Distributor: Cold Spring Harbor Laboratory Label: Cold Spring Harbor Laboratory Section: New Results Type: article.

[28] Kai W. Wirtz. A generic model for changes in microbial kinetic coefficients. *Journal of Biotechnology*, 97(2):147–162, August 2002.

[29] Don K. Button. Affinity of organisms for substrate. *Limnology and Oceanography*, 31:435–456, 1986.

[30] R. V. O'Neill, D. L. DeAngelis, J. J. Pastor, B. J. Jack-

son, and W. M. Post. Multiple nutrient limitations in ecological models. *Ecol Modelling*, 46:147–163, 1989.

[31] J. L. Snoep, M. Mrwebi, J. M. Schuurmans, J. M. Rohwer, and M. J.YR 2009 Teixeira de Mattos. Control of specific growth rate in Saccharomyces cerevisiae. *Microbiology*, 155(5):1699–1707, 2009. Publisher: Microbiology Society,.

[32] S. Sharma and R. Steuer. Modelling microbial communities using biochemical resource allocation analysis. *J R Soc Inter*, 16:20190474, 2019.

[33] R. H. MacArthur. Species packing and competitive equilibria for many species. *Theor Pop Biol*, 1:1–11, 1970.

[34] F. F. Blackman. Optima and limiting factors. *Annals of Botany*, 19:281–295, 1905.

[35] J. R. Casey and M. J. Follows. A steady-state model of microbial acclimation to substrate limitation. *PLoS Comput Biol*, 16:e1008140, 2020.

[36] M. R. Droop. Some thoughts on nutrient limitation in algae. *Journal of Phycology*, 9:264–272, 1973.

[37] U. Sommer. A comparison of the droop and the monod models of nutrient limited growth applied to natural populations of phytoplankton. *Funct Ecol*, 5:535–544, 1991.

[38] W. G. Sunda, K. W. Shertzer, and D. R. Hardison. Ammonium uptake and growth models in marine diatoms: Monod and Droop revisited. *Mar Ecol Prog Ser*, 386:29–41, 2009.

[39] H. Wang, P. V. Garcia, S. Ahmed, and C. M. Heggerud. Mathematical comparison and empirical review of the Monod and Droop forms for resource-based population dynamics. *Ecol Model*, 466:109887, 2022.

[40] L. Von Bertalanffy. Quantitative laws in metabolism and growth. *Q Rev Biol*, 32:217–231, 1957.

[41] E. Sperfeld, D. Martin-Creuzburg, , and A. Wacker. Multiple resource limitation theory applied to herbivorous consumers: Liebig's minimum rule vs. interactive co-limitation. *Ecol Lett*, 15:142–150, 2012.

[42] S. F. M. Hart, D. Skelding, A. J. Waite, J. C. Burton, and W. Shou. High-throughput quantification of microbial birth and death dynamics using fluorescence microscopy. *Quant Biol*, 7:69–81, 2019.

[43] C. S. Holling. Some characteristics of simple types of predation and parasitism i. *The Canadian Entomologist*, 91:358–369, 1959.

[44] Naomi Ziv, Mark L. Siegal, and David Gresham. Genetic and Nongenetic Determinants of Cell Growth Variation Assessed by High-Throughput Microscopy. *Molecular Biology and Evolution*, 30(12):2568–2578, December 2013.

[45] J.D. Owens and J.D. Legan. Determination of the Monod substrate saturation constant for microbial growth. *FEMS Microbiology Letters*, 46(4):419–432, October 1987.

[46] H W Jannasch. Growth characteristics of heterotrophic bacteria in seawater. *Journal of Bacteriology*, 95(2):722–723, February 1968.

[47] Karin Kovárová-Kovar and Thomas Egli. Growth kinetics of suspended microbial cells: From single-substrate-controlled growth to mixed-substrate kinetics. *Microbiology and Molecular Biology Reviews*, 62:646–666, 1998.

[48] Ron Milo and Rob Phillips. *Cell Biology by the Numbers*. Garland Science, Taylor Francis Group, 2016.

[49] Thomas Ferenci. 'growth of bacterial cultures' 50 years on: Towards an uncertainty principle instead of constants in bacterial growth kinetics. *Research in Microbiology*, 150:431–38, 1999.

[50] Huai-Feng Liu, Ben-Hong Wu, Pei-Ge Fan, Shao-Hua Li, , and Lian-Sheng Li. Sugar and acid concentrations in 98 grape cultivars analyzed by principal component analysis. *Journal of the Science of Food and Agriculture*, 86:1526—36, 2006.

[51] Zerihun T.Dame, Farid Aziat, Rupasri Mandal, Ram Krishnamurthy, and Souhaila Bouatra et al. The human saliva metabolome. *Metabolomics*, 11:1864–83, 2015.

[52] Tim N. Enke, Manoshi S. Datta, Julia Schwartzman, nathan Cermak, Désirée Schmitz, Julien Barrere, Alberto Pascual-García, and Otto X. Cordero. Modular assembly of polysaccharide-degrading marine microbial communities. *Current Biology*, 29, 2019.

[53] Jonas Cremer, Markus Arnoldini, and Terence Hwa. Effect of water flow and chemical environment on microbiota growth and composition in the human colon. *Proceedings of the National Academy of Sciences*, 114:6438—-43, 2017.

[54] J. E. Barrick and R. E. Lenski. Genome dynamics during experimental evolution. *Nat Rev Genet*, 14:827–839, 2013.

[55] Chevin Luis-Miguel. On measuring selection in experimental evolution. *Biology Letters*, 7(2):210–213, April 2011.

[56] Michael Manhart, Bharat V. Adkar, and Eugene I. Shakhnovich. Trade-offs between microbial growth phases lead to frequency-dependent and non-transitive selection. *Proceedings of the Royal Society B: Biological Sciences*, 285(1872):20172459, February 2018. Publisher: Royal Society.

[57] E. Atolia, S. Cesar, H. A. Arjes, M. Rajendram, H. Shi, B. D. Knapp, S. Khare, A. Aranda-Díaz, R. E. Lenski, and K. C. Huang. Environmental and physiological factors affecting high-throughput measurements of bacterial growth. *mBio*, 11:e01378–20, 2020.

[58] Richard E. Lenski, Michael R. Rose, Suzanne C. Simpson, and Scott C. Tadler. Long-Term Experimental Evolution in Escherichia coli. I. Adaptation and Divergence During 2,000 Generations. *The American Naturalist*, 138(6):1315–1341, December 1991.

[59] J. H. Gillespie. Molecular evolution over the mutational landscape. *Evolution*, 38:1116–1129, 1984.

[60] G. I. Lang, D. P. Rice, M. J. Hickman, E. Sodergren, G. M. Weinstock, D. Botstein, and M. M. Desai. Pervasive genetic hitchhiking and clonal interference in forty evolving yeast populations. *Nature*, 500:571–574, 2013.

[61] Anat Bren, Yuval Hart, Erez Dekel, Daniel Koster, and Uri Alon. The last generation of bacterial growth in limiting nutrient. *BMC Systems Biology*, 7(1):27, March 2013.

[62] Thomas Ferenci. Adaptation to life at micromolar nutrient levels: The regulation of escherichia coli glucose transport by endoinduction and camp. *FEMS Microbiology Reviews*, 18:301–317, 1996.

[63] J. W. Lengeler. Carbohydrate transport in bacteria under environmental conditions, a black box? *Antonie van Leeuwenhoek*, 63, 1993.

[64] J. F. Crow and M. Kimura. *An Introduction to Population Genetics Theory*. Harper and Row, New York, 1970.

[65] B. Charlesworth. Effective population size and patterns of molecular evolution and variation. *Nat Rev Genet*, 10:195–205, 2009.

[66] O. Hallatschek, P. Hersen, S. Ramanathan, and D. R. Nelson. Genetic drift at expanding frontiers promotes

gene segregation. *Proc Natl Acad Sci USA*, 104:19926–19930, 2007.

[67] M. Shpak. Selection against demographic stochasticity in age-structured populations. *Genetics*, 177:2181–2194, 2007.

[68] J. H. Gillespie. Natural selection for within-generation variance in offspring number II. Discrete haploid models. *Genetics*, 81:403–413, 1975.

[69] M. Kimura. *The Neutral Theory of Molecular Evolution*. Cambridge University Press, Cambridge, 1983.

[70] A. W. R. Serohijos and E. I. Shakhnovich. Merging molecular mechanism and evolution: Theory and computation at the interface of biophysics and evolutionary population genetics. *Curr Opin Struct Biol*, 26:84–91, 2014.

[71] M. Lynch and K. Hagner. Evolutionary meandering of intermolecular interactions along the drift barrier. *Proc Natl Acad Sci USA*, 112:E30–38, 2015.

[72] W. J. Ewens. *Mathematical Population Genetics*. Springer-Verlag, New York, 2004.

[73] R. E. Lenski, M. R. Rose, S. C. Simpson, and S. C. Tadler. Long-term experimental evolution in Escherichia coli. I. Adaptation and divergence during 2,000 generations. *Am Nat*, 138:1315–1341, 1991.

[74] Karin Elbing, Christer Larsson, Roslyn M. Bill, Eva Albers, Jacky L. Snoep, Eckhard Boles, Stefan Hohmann, and Lena Gustafsson. Role of Hexose Transport in Control of Glycolytic Flux in Saccharomyces cerevisiae. *Applied and Environmental Microbiology*, 70(9):5323–5330, September 2004. Publisher: American Society for Microbiology.

[75] K. Gomez, J. Bertram, and J. Masel. Directional selection rather than functional constraints can shape the G matrix in rapidly adapting asexuals. *Genetics*, 211:715–729, 2019.

[76] Jie Lin, Michael Manhart, and Ariel Amir. Evolution of Microbial Growth Traits Under Serial Dilution. *Genetics*, May 2020. Publisher: Genetics Section: Investigation.

[77] Gregory J. Velicer and Richard E. Lenski. Evolutionary trade-offs under conditions of resource abundance and scarcity: Experiments with bacteria. *Ecology*, 80:1168–1179, 1999.

[78] M. Kaspari and J. S. Powers. Biogeochemistry and geographical ecology: embracing all twenty-five elements required to build organisms. *Am Nat*, 188:S62–S73, 2016.

[79] S. J. Gould and R. C. Lewontin. The spandrels of San Marco and the Panglossian paradigm: A critique of the adaptationist programme. *Proc R Soc B*, 205:581–598, 1979.

[80] P. J. Gerrish and R. E. Lenski. The fate of competing beneficial mutations in an asexual population. *Genetica*, 102/103:127–144, 1998.

[81] S. Schiffels, G. J. Szöllösi, V. Mustonen, and M. Lässig. Emergent neutrality in adaptive asexual evolution. *Genetics*, 189:1361–1375, 2011.

[82] M. Kimura and T. Ohta. The average number of generations until fixation of a mutant gene in a finite population. *Genetics*, 61:763–771, 1969.

[83] M. Manhart and E. I. Shakhnovich. Growth tradeoffs produce complex microbial communities on a single limiting resource. *Nat Commun*, 9:3214, 2018.

[84] S. J. Schink, E. Biselli, C. Ammar, and U. Gerland. Death rate of E. coli during starvation is set by maintenance cost and biomass recycling. *Cell Syst*, 9:64–73, 2019.

[85] P. van Bodegom. Microbial maintenance: A critical review on its quantification. *Microb Ecol*, 53:513–523, 2007.

[86] Motoo Kimura. On the Probability of Fixation of Mutant Genes in a Population. *Genetics*, 47(6):713–719, June 1962. Publisher: Genetics Section: INVESTIGATIONS.

[87] Jacques Monod and A Audureau. Mutation et adaptation enzymatique chez escherichia coli-mutabile. In *Annales de l'Institut Pasteur*, volume 72, pages 868–878. Masson Editeur 120 Blvd Saint-Germain, 75280 Paris 06, France, 1946.

[88] Evelyn M Witkin. Inherited differences in sensitivity to radiation in escherichia coli. *Proceedings of the National Academy of Sciences of the United States of America*, 32(3):59, 1946.

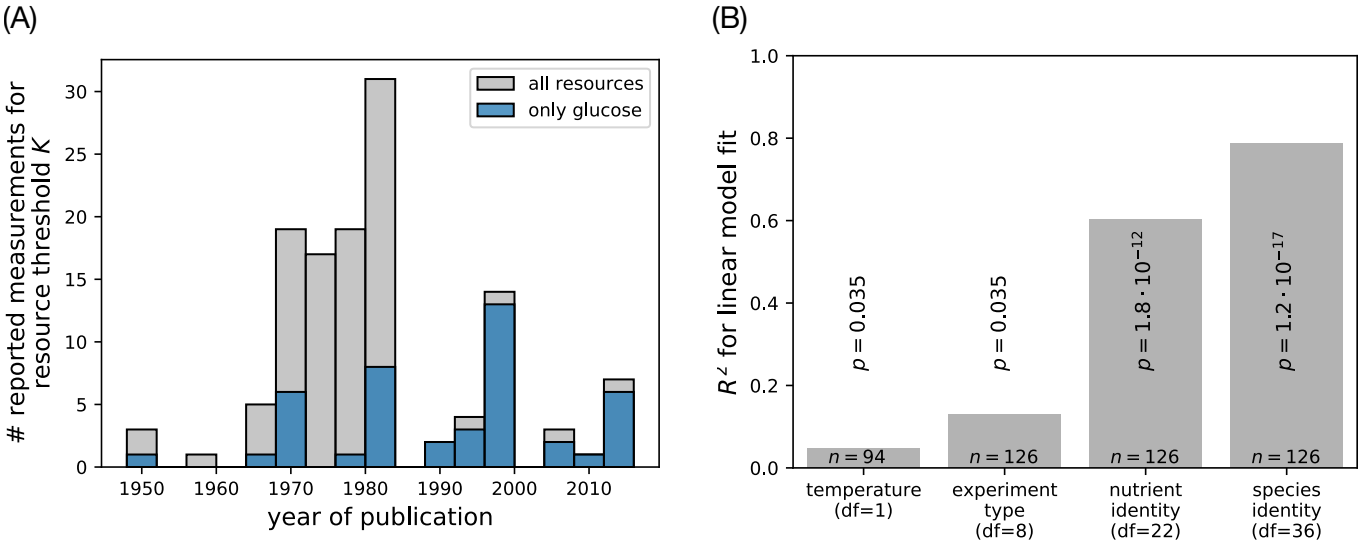

FIG. S1. **Historical trends and technical covariates of measured resource thresholds.** (A) The number of measured resource thresholds K published in peer-reviewed journals aggregated by year, based on our literature collection (Supplementary Data Table 1). The subset of measurements with glucose as the limiting resource are shown in blue. (B) Linear regressions of technical covariates against thresholds $\log_{10} K$, with degrees of freedom (df), number of data points (n), and p-values indicated.

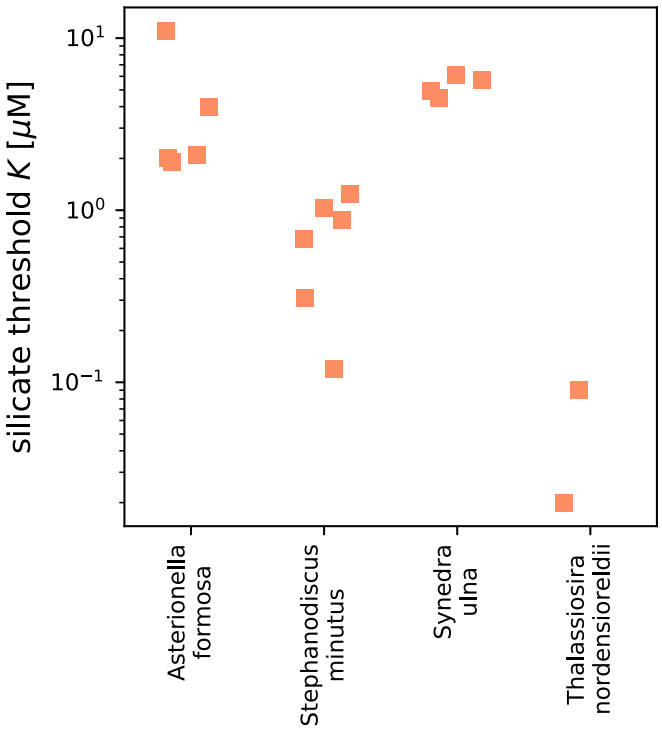

FIG. S2. **Silicate thresholds across taxa.** Subset of data from Fig. 2A for silicate; only organisms with more than one measurement are shown. Marker color and shape are the same as in Fig. 2A.

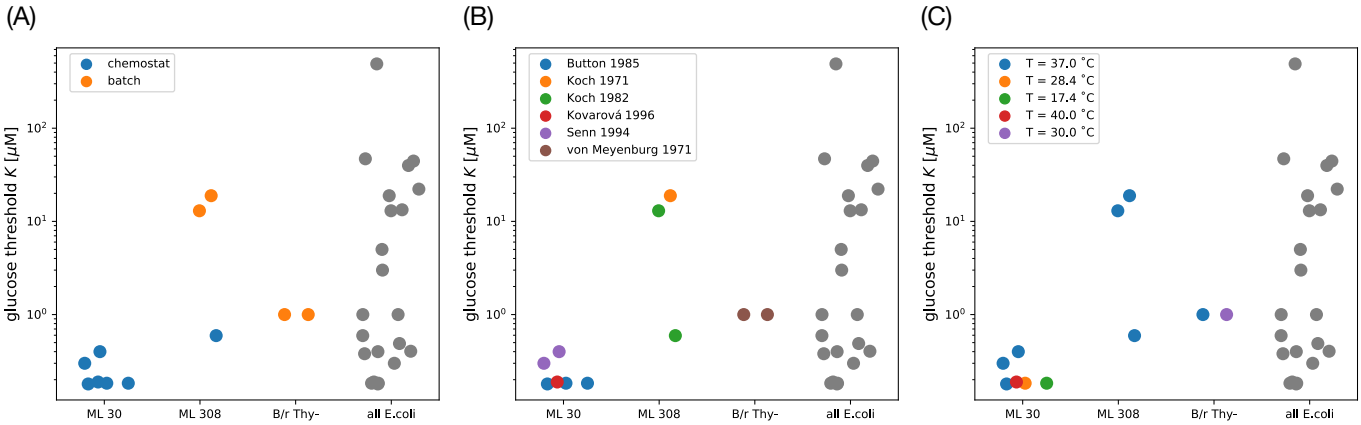

FIG. S3. **Variation in *E. coli* glucose thresholds broken down by strain.** Subset of data from Fig. 2A for *E. coli* on glucose, with different strains separated. The strains ML 30 and ML308 were derived from a natural isolate in human feces by Jacques Monod in 1946 and differ in their genes for lactose utilization [87]: the lacI repressor is non-functional in ML308. The strain B/r Thy- is auxotrophic for thymine and derived from *E. coli* B/r, a strain isolated in radiation experiments by Witkin [88]. We only show substrains with two or more measurements from the dataset. The three panels show the same data but are colored according to (A) experimental method (batch or chemostat), (B) publication, and (C) temperature.

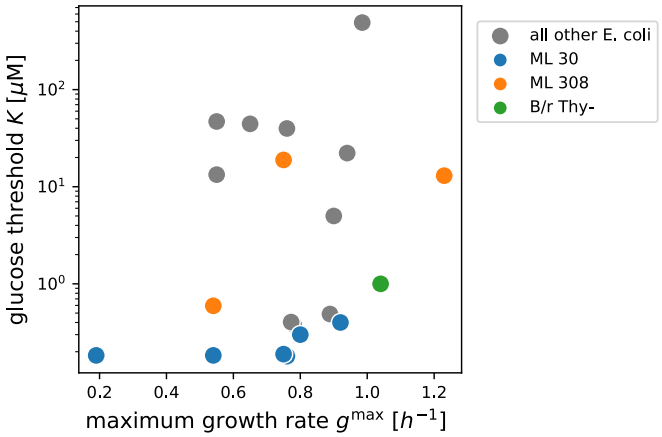

FIG. S4. **Correlation in *E. coli* glucose thresholds and maximum growth rate broken down by strain.** Subset of data from Fig. 2D for *E. coli* on glucose, with strains labeled by different colors. Highlighted strains are the same as in Fig. S3.

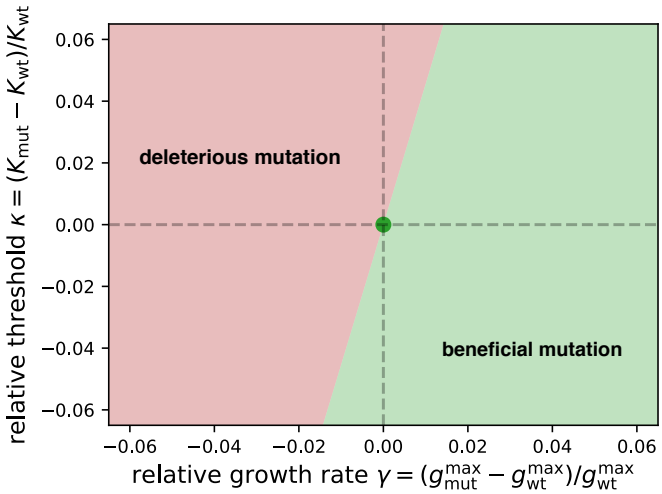

FIG. S5. **Diagram of selection across mutation effects under batch growth.** The space of mutation effects on maximum growth rate $\gamma = (g_{\rm mut}^{\rm max} - g_{\rm wt}^{\rm max})/g_{\rm wt}^{\rm max}$ and resource threshold $\kappa = (K_{\rm mut} - K_{\rm wt})/K_{\rm wt}$ relative to a wild-type strain (central dot), with green marking the space of mutations that are overall beneficial ($s > 0$) and red marking mutations that are overall deleterious ($s < 0$) according to Eq. (4).

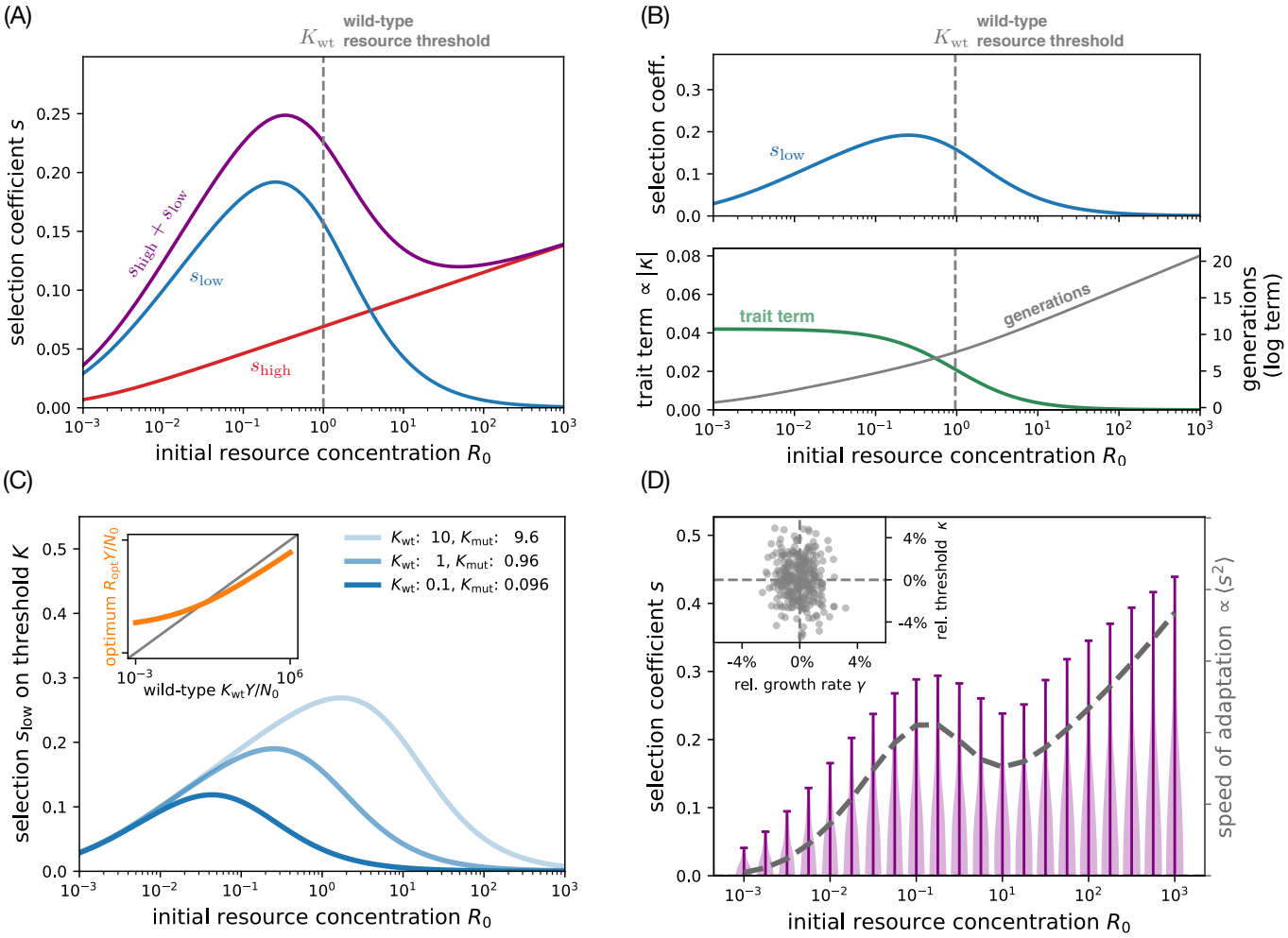

FIG. S6. **Selection dependence on resource concentration under fixed-bottleneck batch dynamics.** (A) Dependence on external resource concentration R_0 of the total selection coefficient (purple) and its two components at high (s_{high}, red) and low (s_{low}, blue) resource concentrations under a fixed bottleneck (Eq. (4)). (B) Selection s_{low} on growth at low resource concentrations (top panel) decomposed into two constituent factors (bottom panel) at fixed bottleneck biomass ($N_0 = 10^{-3}$). The top panel is the same as panel A for the approximate selection coefficient s_{low}; in the bottom panel, the two factors that constitute s_{low} with the trait factor from Eq. (S45) in green and the log term from Eq. (S46) in gray. The log term is related but not identical to the number of generations in the growth cycle. Panel A and B are based on an example mutation pair with relative effect $\gamma = 0.01$ on maximum growth rate and $\kappa = -0.04$ on resource threshold over the wild-type traits $g_{\text{wt}} = 1$ and $K_{\text{wt}} = 1$ with equal yield. (C) Selection on the threshold K as a function of resource concentration R_0 for three different values of K (different shades of blue). The inset shows a numerical calculation (orange points) of the optimal resource concentration R_{opt} that maximizes selection on K as a function of the wild-type threshold K_{wt}; the gray line is the identity. Parameters are the same as in Panel A and B, but we include two alternative wild-type resource thresholds $K_{\text{wt}} = 10$ (light blue) and $K_{\text{wt}} = 0.1$ (dark blue). (D) The distribution of beneficial selection coefficients (purple) as a function of initial resource concentration R_0, with the variance (which is proportional to the speed of adaptation) shown in the dashed gray line and plotted against the right axis. The inset shows the underlying sample of mutations according to their relative effects on maximum growth rate γ and resource threshold κ. We sample the effect of mutation independently from a Gaussian distribution for γ (mean $\mu = 0$, s.d. $\sigma = 0.01$) and κ (mean $\mu = 0$, s.d. $\sigma = 0.02$). All panels assume initial population biomass $N_0 = 0.001$, initial mutant frequency $x = 0.01$ and equal yield for mutant and wild-type.

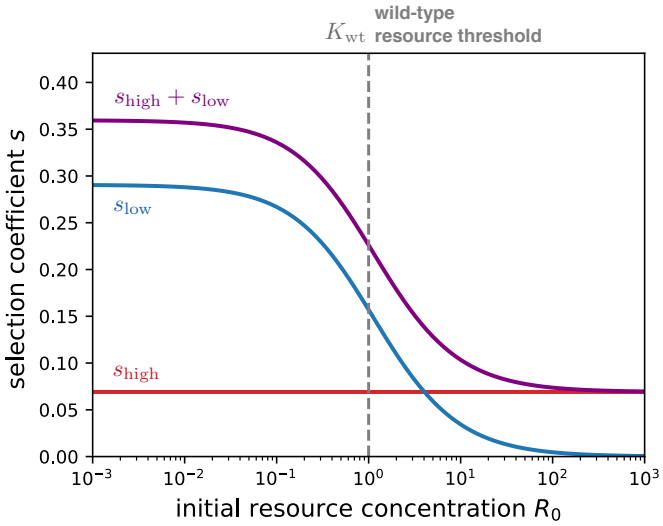

FIG. S7. **Selection dependence on resource concentration under fixed-dilution batch dynamics.** Same as Fig. S6A, but for fixed-dilution batch dynamics with $D = 1000$.

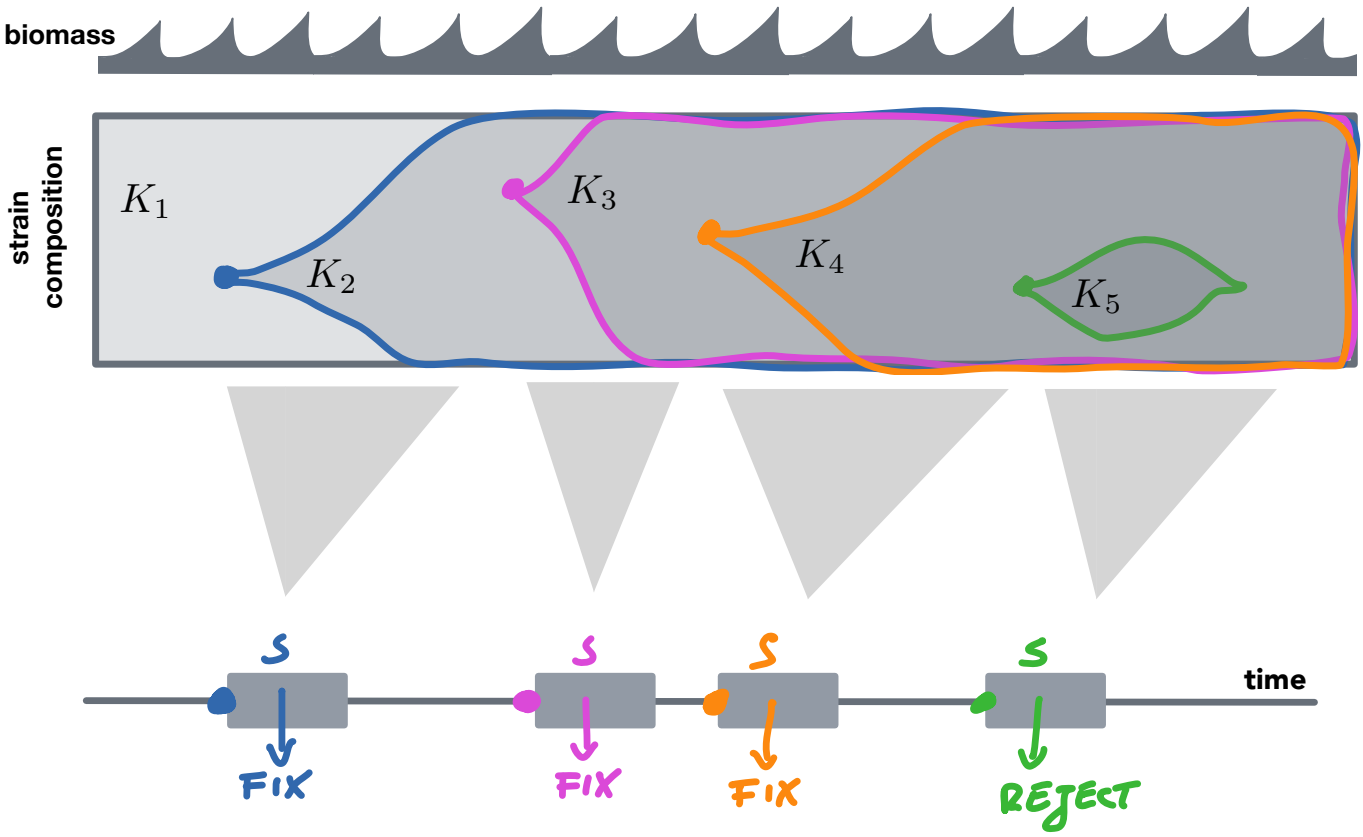

FIG. S8. **Schematic of evolutionary dynamics in the strong-selection weak-mutation (SSWM) regime.** Top panel shows a schematic of the population biomass undergoing cycles of batch dynamics with serial transfers. The middle panel shows the genetic composition of the population. The population begins with a resource threshold K_1. Then a mutation arises with a different threshold K_2 (blue), which increases in frequency until it fixes. Then another mutation with a threshold K_3 arises (magenta), and the process continues. The bottom panel shows a simplified algorithm for this process that we use in our simulations (Methods), where mutations are determined to fix or go extinct one at a time based on their selection coefficients, without explicitly simulating their intermediate frequency dynamics.

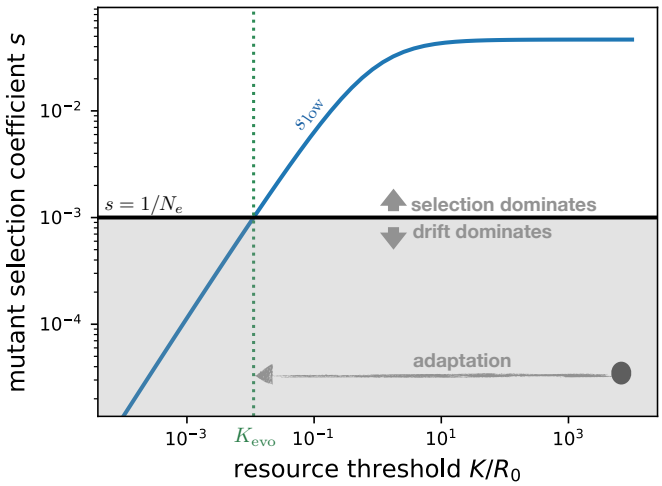

FIG. S9. **Selection-drift balance under fixed-bottleneck batch dynamics.** Selection on the resource threshold K as a function of the current background value of the trait in the population (blue line, Eq. (4)), with mutation effect $\kappa = -10^{-2}$. The horizontal black line marks the strength of genetic drift; its intersection with the selection coefficient defines the value of K at which selection-drift balance occurs (vertical dotted line). Above this point, selection is stronger than genetic drift, and so the resource threshold will adapt downward until it reaches that point. Parameters are $R_0 = 1$, $N_0 = 0.01$, $N_{\rm e} = 10^3$ and $x = 0.001$. We set mutant and wild-type to equal maximum growth rate and equal yield.

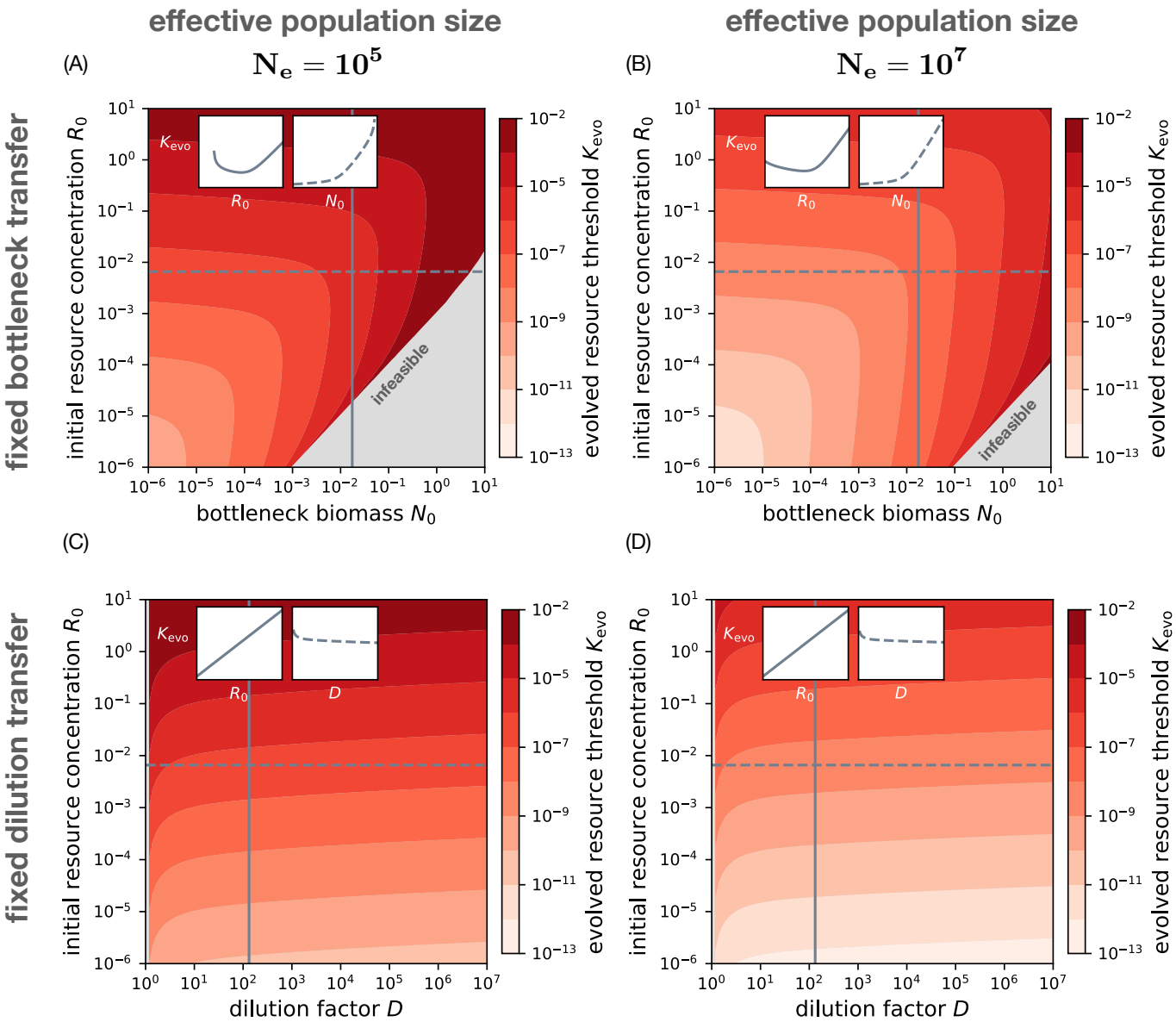

FIG. S10. **The evolved resource threshold as a function of experimental parameters with independent genetic drift.** (A) We numerically solve for the evolved resource threshold $K_{\rm evo}$ under selection-drift balance (using Eqs. (4) and (6)) as a function of the fixed-bottleneck biomass N_0 and initial resource concentration R_0, where the effective population size $N_{\rm e} = 10^5$ is an independent parameter. Where the selection-drift balance condition is infeasible (gray area), the resource threshold evolves neutrally without steady state. The insets show cross-sections along initial resource concentration R_0 (solid line) and bottleneck biomass N_0 (dashed line). (B) Same as panel A, but for a larger effective population size $N_{\rm e} = 10^7$. (C) Same as panel A but for fixed-dilution batch dynamics, with varying D instead of N_0. (D) Same as panel C, but for a larger effective population size $N_{\rm e} = 10^7$. All panels use identical growth rate $g^{\rm max} = 1$ and biomass yield $Y = 1$ for wild-type and mutant strain with a fixed mutation effect $\kappa = 0.01$ on the resource threshold. The initial mutant frequency $x = 1/N_{\rm e}$ is adjusted to the effective population size $N_{\rm e}$.

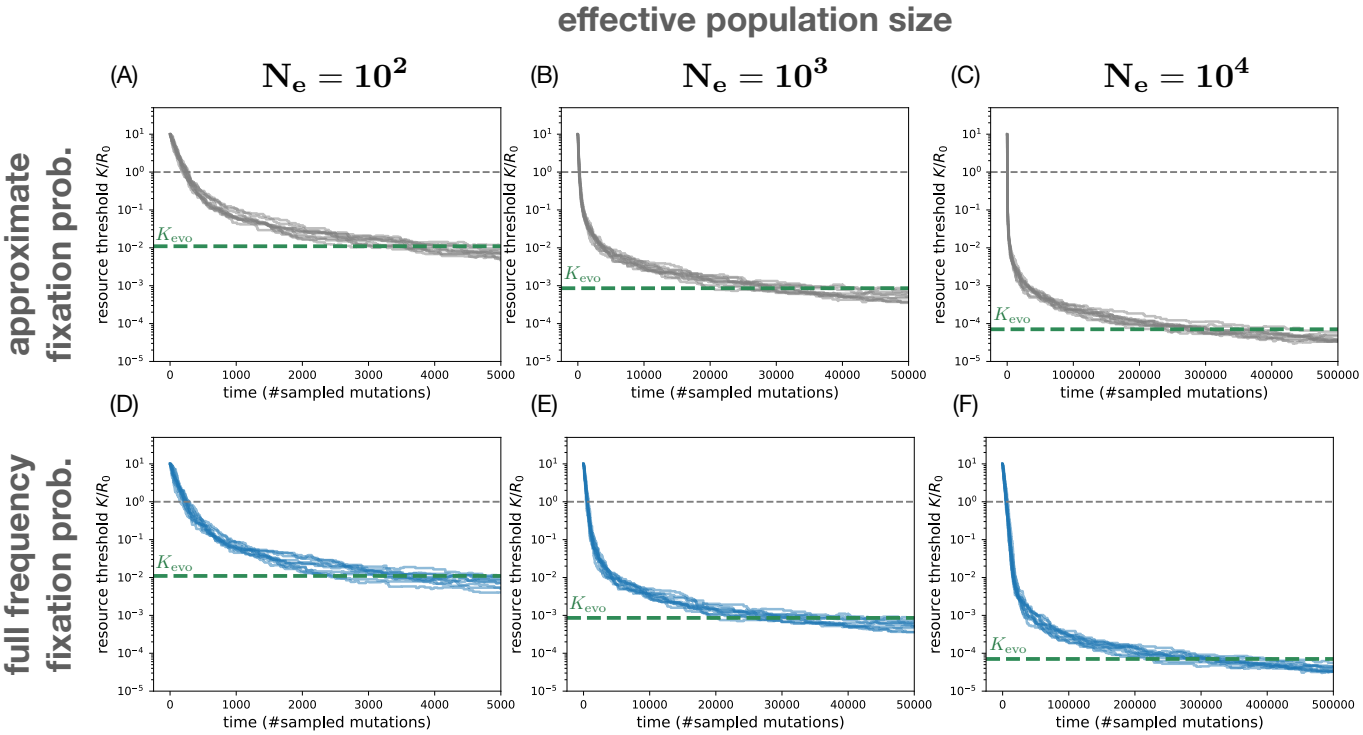

FIG. S11. **Simulated evolutionary trajectories of the resource threshold under batch dynamics.** We simulate the time-course of resource threshold evolution in the SSWM regime (Methods) for different strengths of genetic drift ($1/N_e$). Each line corresponds to a separate run of the stochastic evolution process. Here mutations are sampled with random effect $\kappa = (K_{mut} - K_{wt})/K_{wt}$ from a uniform distribution in $[-0.1, 0.1]$ and accepted or rejected according to their probability of fixation (Methods). (A)-(C) In the top row, we use the approximate fixation probability Eq. (S48) which is based on the selection coefficient at the initial mutant frequency $x = 1/N_e$. (D)-(F) In the bottom row, we use the integrated form of the fixation probability from Eq. (S47) that takes into account the frequency-dependence of the mutant selection coefficient. For each panel, we numerically calculate the resource threshold K_{evo} at selection-drift balance (orange line) using Eqs. (4) and (6). To guide the eye, we also mark the resource threshold $K = R_0$ that matches the environmental concentration (gray line). All panels are based on identical maximum growth rate $g^{max} = 1$ and biomass yield $Y = 1$ for the mutant and wild-type strain such that only the resource threshold evolves. The length of the growth cycle is constant with ≈ 6.6 generations at initial resource concentration $R_0 = 1$ and fixed bottleneck biomass $N_0 = 0.01$.

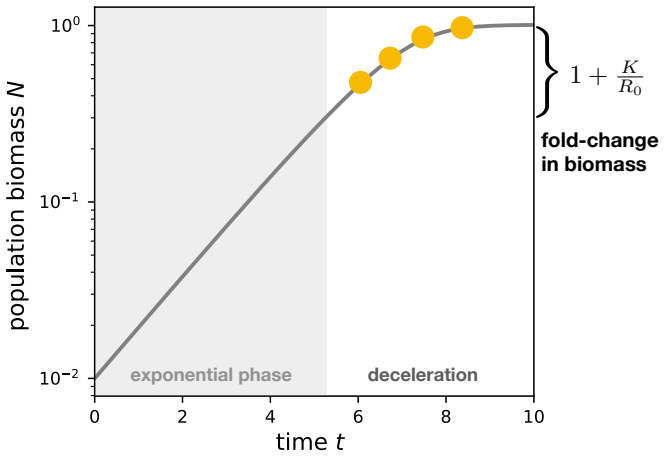

FIG. S12. **Detecting the resource threshold K from time-series data.** We use an initial resource concentration $R_0 = 10$ close to the resource threshold of the wild-type strain ($K_{wt} = 5$, see Fig. 1) to simulate a monoculture growth curve from Eq. (8) (Methods). The population leaves steady exponential growth phase (gray area) to enter deceleration (white area). To fit the resource threshold K, the time-series must include multiple data points in the deceleration phase (orange dots). On the right axis, a bracket marks the fold-change from the onset of deceleration at biomass to the saturation.

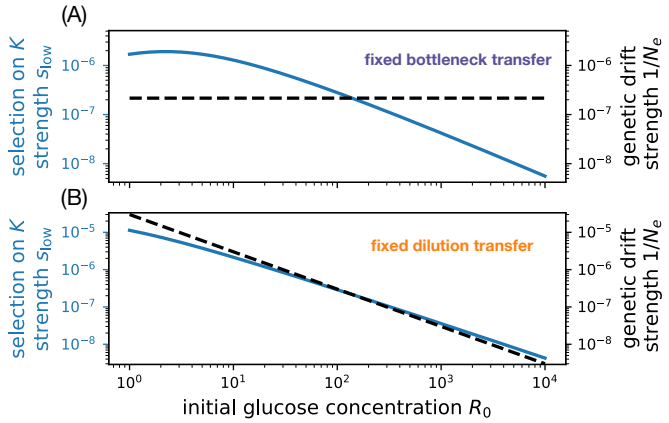

FIG. S13. **Environmental dependence of selection and genetic drift under batch dynamics.** The top panel shows selection s_{low} on the threshold K (blue solid line, left axis) and the strength of genetic drift $1/N_{\text{e}}$ (dashed black line, right axis) as functions of the resource concentration R_0 under fixed-bottleneck batch dynamics. In this case, the effective population size is an independent parameter of the resource concentration. We use parameters based on the LTEE (same as in Fig. 4C): $N_0 = 4.6 \cdot 10^5$ cells/mL and $N_{\text{e}} = V \cdot N_0$ using culture volume $V = 10$ mL, $g^{\max} = 0.888$/h, and $Y = 3.3 \cdot 10^8$ cells/μmol [22]. The bottom panel shows the same but for fixed-dilution batch dynamics, with $D = 100$; in this case the effective population size is proportional to the resource concentration, and thus the strength of genetic drift decreases with R_0.

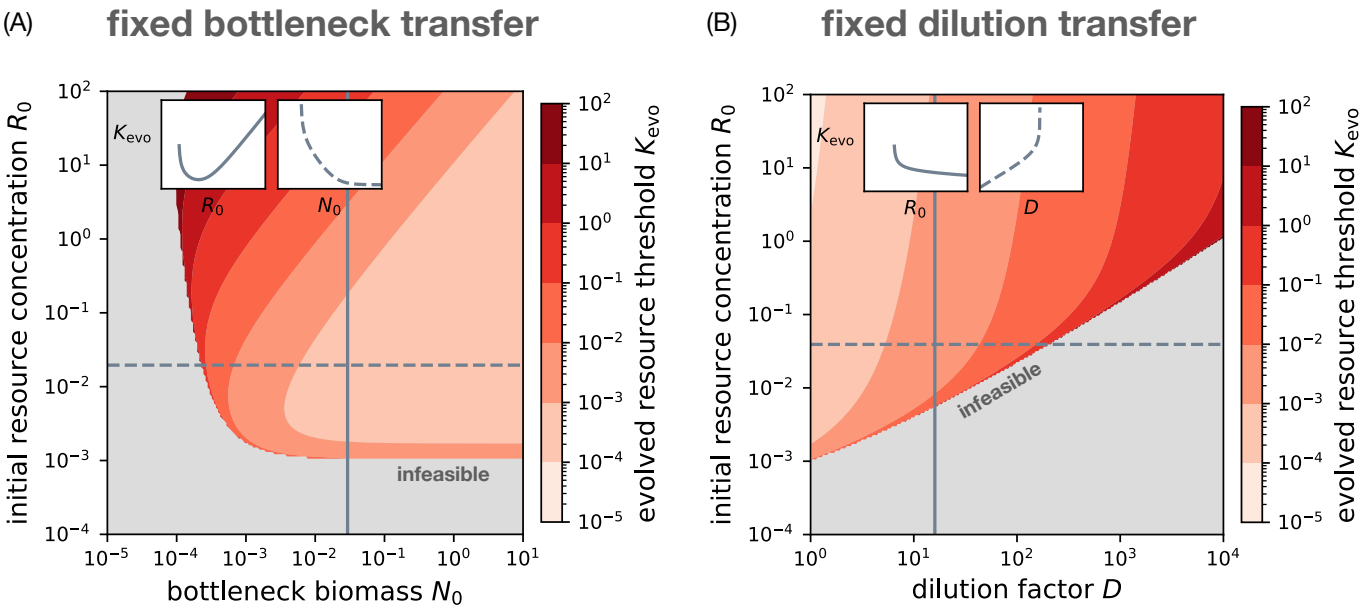

FIG. S14. **The evolved resource threshold as a function of experimental parameters under coupled genetic drift.** (A) Same as Fig. S10A, but where the effective population size N_{e} is proportional to the biomass bottleneck N_0 as in well-mixed laboratory experiments with fixed-bottleneck batch dynamics. We set $N_{\text{e}} = N_0 \cdot V$, where $V = 10^5$ is the culture volume such that a bottleneck biomass of $N_0 = 0.01$ corresponds to an effective population size of $N_{\text{e}} = 10^3$ cells. (B) Same as panel A but for fixed-dilution batch dynamics, where the effective population size is $N_{\text{e}} = N_0 \cdot V = V R_0 Y/(D-1)$.

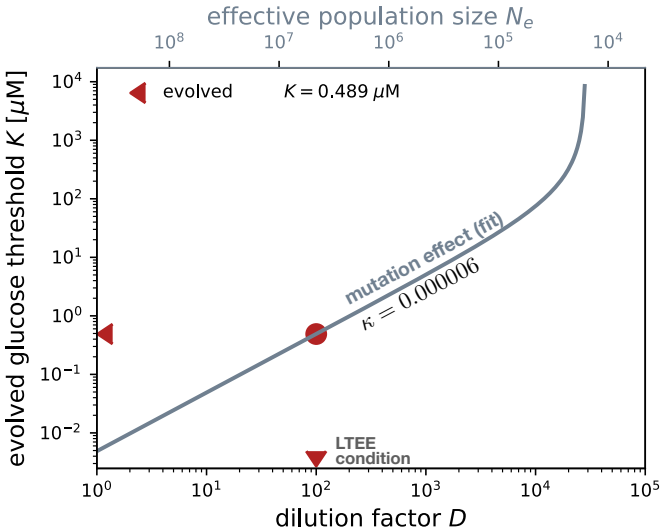

FIG. S15. **Inferred mutation effect for the Long-Term Evolution Experiment.** Evolved glucose threshold K_{evo} as a function of the dilution factor D under fixed-dilution batch dynamics. If we assume the glucose threshold for *E. coli* in the LTEE is under selection-drift balance, then we can use this dependence to infer the value of the mutation effect κ that would be consistent with the other known parameters of the system. We numerically solve for selection-drift balance using Eqs. (4) and (6) with dilution factor $D = 100$, initial glucose concentration $R_0 = 139$ μM, and evolved resource threshold $K = 0.489$ μM (red dot). We obtain an estimate of $\kappa = 6 \cdot 10^{-6}$.

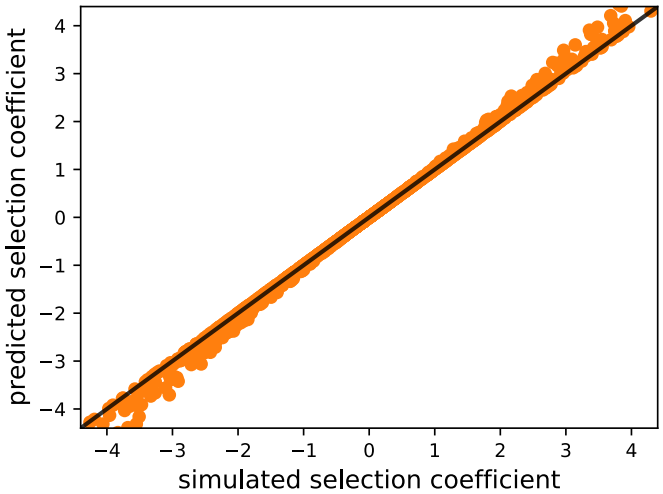

FIG. S16. **Test of the selection coefficient approximation.** The predicted selection coefficient across a sample of wild-type and mutant strains, compared to the selection coefficient from simulation of the differential equations. The black diagonal line indicates perfect agreement between simulation and prediction. We draw the background wild-type traits over four orders of magnitude and sample relative mutant effects on maximum growth rate, resource threshold and cell yield from a rectangular region in trait space: $[-0.5, 0.5]^3$. Each strain pair is systematically evaluated at different frequencies $x = 0.01, 0.5, 0.99$ using the general Eq. (S32) and contributes three data points. Without loss of generality we normalize the initial biomass to $N_0 = 0.01$ and initial resource concentration to $R_0 = 1$. The trait values for the resource threshold span two orders of magnitude around this concentration such that we cover both limiting scenarios with dominant selection on maximum growth rate ($R_0 \gg K_1$) and resource threshold ($R_0 \ll K_1$).

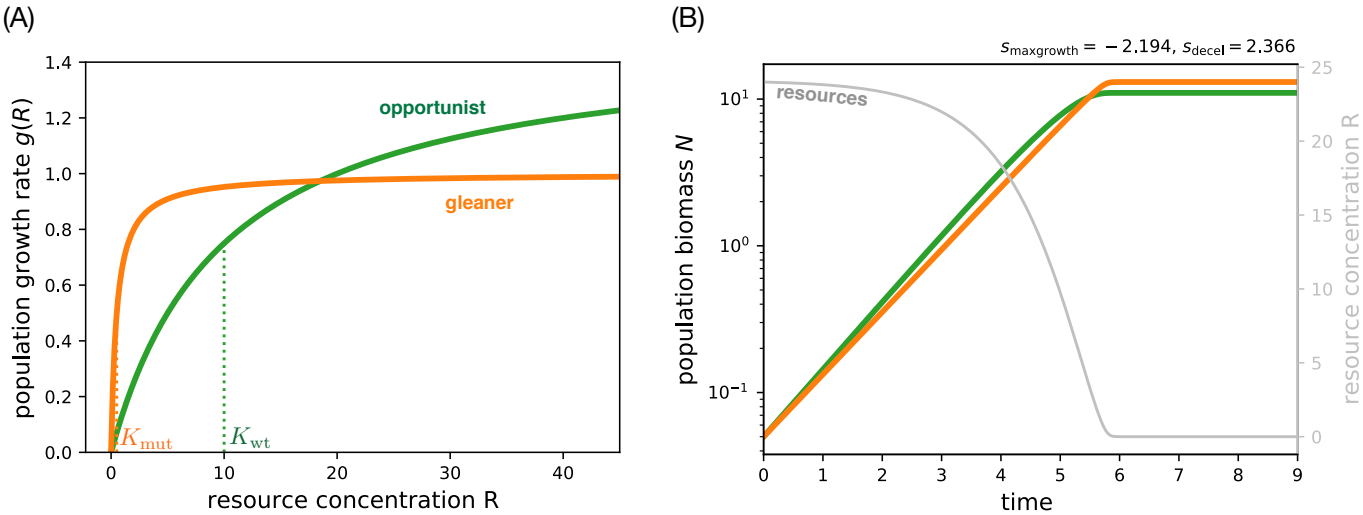

FIG. S17. **The gleaner and opportunity strategy in the Monod growth model.** (A) The growth rate $g(R)$ as a function of the external resource concentration R for two strains with a tradeoff. The opportunist strain (green) has a higher maximum growth rate $g^{\max} = 1.5$ compared to the gleaner strain (orange) with $g^{\max} = 1$. But the gleaner has the growth rate advantage at low concentrations due to a smaller resource threshold $K = 0.5$ (orange dotted line, not visible) relative to the opportunist with $K = 10$ (green dotted line). (B) A single growth cycle for the gleaner and opportunist strain pair from panel A. We simulate the population dynamics according to Eq. (8), starting from an initial mutant frequency $x = 0.5$ and total initial biomass $N_0 = 0.01$. On a separate axis, the transient resource concentration R (gray line, initial value $R_0 = 24$) and in the panel title, the components of selection as computed from the equation Eq. (4).

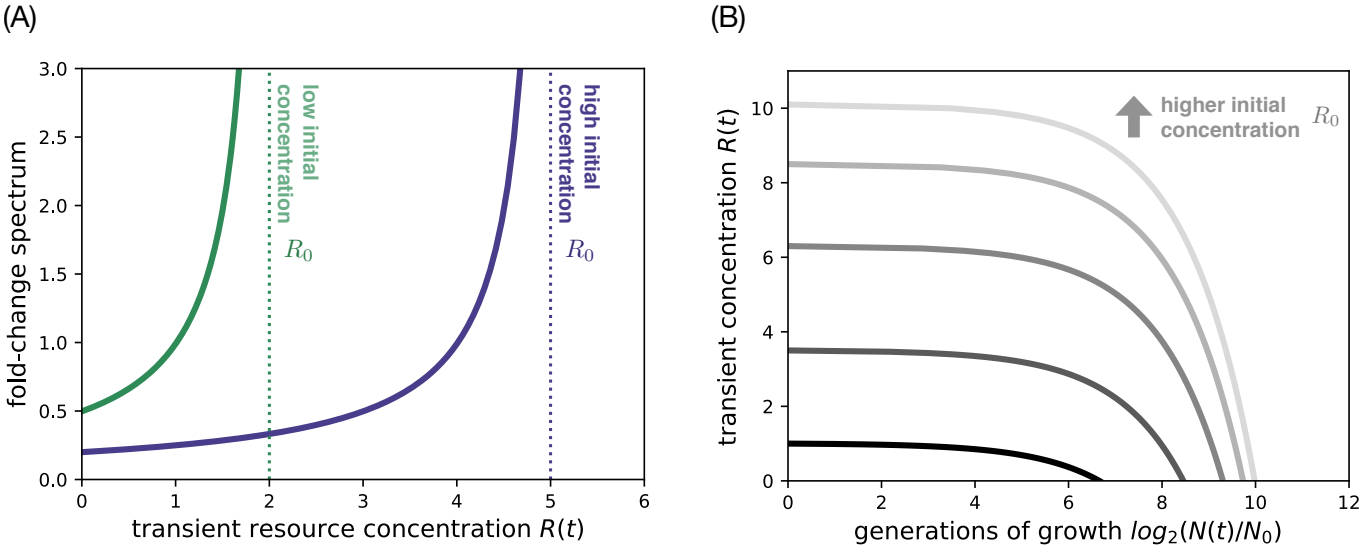

FIG. S18. **Selection within a batch growth cycle.** (A) The fold-change spectrum (thick lines) throughout the growth cycle for high and low initial concentration R_0 (dotted lines). Curves are computed from the weight term in Eq. (S27) with effective biomass yield $\bar{Y} = 1$ and $N_0 = 0.01$. (B) The transient resource level for increasing initial concentration of resource (gray lines). The dashed horizontal line is the critical resource concentration Z for the same pair of strains shown in Fig. 1A at equal frequency $x = 0.5$. The lowest line ($R_0 = 1$) corresponds to the resource trajectory for the selection scenario used for the phase diagram in Fig. S5. The transient resources are converted into generations using the equations for resource consumption, assuming an identical biomass yield $Y = 1$ for both strains and initial biomass $N_0 = 0.01$.

Supplementary Information: Microbial population dynamics decouple nutrient affinity from environmental concentration

Justus Wilhelm Fink*
Institute of Integrative Biology, Department of Environmental Systems Science, ETH Zurich, Zurich, Switzerland

Noelle A. Held
Institute of Biogeochemistry and Pollutant Dynamics, Department of Environmental Systems Science, ETH Zurich, Zurich, Switzerland and Department of Environmental Microbiology, Swiss Federal Institute of Aquatic Science and Technology (Eawag), Dübendorf, Switzerland

Michael Manhart†
Institute of Integrative Biology, Department of Environmental Systems Science, ETH Zurich, Zurich, Switzerland Department of Environmental Microbiology, Swiss Federal Institute of Aquatic Science and Technology (Eawag), Dübendorf, Switzerland and Center for Advanced Biotechnology and Medicine and Department of Biochemistry and Molecular Biology, Robert Wood Johnson Medical School, Rutgers University, Piscataway, NJ, USA

(Dated: May 4, 2022)

S1. ALTERNATIVE MODELS OF GROWTH RATE DEPENDENCE ON RESOURCE CONCENTRATIONS

Table S1 lists several common models for growth rate dependence on resource concentration R. Some of these models are mathematically equivalent; for example, Holling [7] proposed a classification scheme for growth models (commonly referred to as Type I, II and III) for the response of predator growth rate on prey density, which exactly corresponds to other models of growth in Table S1. Some of these models are also equivalent in certain limits. At high resource concentrations $R/K \gg 1$, all of the models are approximately equivalent to the constant growth model, since the assumption is that resources are saturating and growth is limited by other processes.

On the other hand, at low concentrations $R/K \ll 1$, the Monod, Blackman, and Bertalanffy models are approximately equivalent to the linear model. We note that a linear model of growth rate on resource concentration leads to logistic density dependence in the population dynamics. Starting from the model of batch-culture growth (Eq. (8)), we can integrate the equation for resource consumption dR/dt to express the current resource concentration $R(t)$ as a function of the biomasses of wild-type N_{wt} and mutant strain N_{mut}:

$$R = R_0 + \frac{N_0}{\bar{Y}} - \frac{N_{\text{wt}}}{Y_{\text{wt}}} - \frac{N_{\text{mut}}}{Y_{\text{mut}}}, \tag{S1}$$

where $\bar{Y}$ is the effective population yield (Table S2). Substituting R from Eq. (S1) into the equations for dN_{wt}/dt and dN_{mut}/dt from Eq. (8) with linear growth rate dependence, we obtain

$$\frac{1}{N_{\text{wt}}}\frac{dN_{\text{wt}}}{dt} = \frac{g_{\text{wt}}^{\max}}{K_{\text{wt}}}\left(R_0 + \frac{N_0}{\bar{Y}} - \frac{N_{\text{wt}}}{Y_{\text{wt}}} - \frac{N_{\text{mut}}}{Y_{\text{mut}}}\right), \tag{S2a}$$

$$\frac{1}{N_{\text{mut}}}\frac{dN_{\text{mut}}}{dt} = \frac{g_{\text{mut}}^{\max}}{K_{\text{mut}}}\left(R_0 + \frac{N_0}{\bar{Y}} - \frac{N_{\text{wt}}}{Y_{\text{wt}}} - \frac{N_{\text{mut}}}{Y_{\text{mut}}}\right). \tag{S2b}$$

This is equivalent to logistic growth for both species or competitive Lotka-Volterra dynamics.

There are also some important differences between models. The Blackman, Monod, Bertalanffy, and Hill models all saturate at high resource concentrations, but the nature of that saturation qualitatively differs. That is, the Monod model converges most slowly due its power law dependence on R. The Hill model also converges as a power law, but assuming $n > 1$, it does so more quickly than Monod. The Bertalanffy model converges even more rapidly due to its exponential dependence on R. Finally, the Blackman model converges to a constant immediately at the threshold concentration $R = K$.

The model most significantly different from the rest is the Droop model, since it depends not on the external resource concentration directly, but only on the resource concentration internal to the cell. Therefore this requires inclusion of a separate resource uptake process to be included in our framework. Under steady-state (chemostat) growth, this will also be equivalent to the Monod model under a shift in the resource concentration parameter $Q - Q_0 \to R$, but under non-steady state conditions (e.g., batch dynamics), the Droop model can differ [12].

* To whom correspondence should be addressed. Email: justus.fink@env.ethz.ch
† To whom correspondence should be addressed. Email: mmanhart@rutgers.edu

model	definition	references
constant	$g(R) = g^{\max}\Theta(R)$	[1–3]
linear	$g(R) = g^{L} \cdot \frac{R}{K}$	[4]
Blackman or Holling Type I	$g(R) = g^{\max} \cdot \left(1 + \left(\frac{R}{K} - 1\right)\Theta(K - R)\right)$	[5–7]
Monod or Holling Type II	$g(R) = g^{\max} \cdot \frac{R}{R+K}$	[7, 8]
Droop (depends on internal concentration Q)	$g(Q) = g^{\max} \cdot \frac{Q-Q_0}{Q}$	[9–12]
Bertalanffy	$g(R) = g^{\max}\left(1 - e^{-R/K}\right)$	[13, 14]
Hill, Moser, or Holling Type III	$g(R) = g^{\max} \cdot \frac{R^n}{R^n+K^n}$	[7, 15, 16]

TABLE S1. **Overview of models for microbial population growth rate.** For each entry, the column "References" lists works that establish or build on the model and have been cited elsewhere in this text. By Θ we mean the Heaviside step function which is 1 for a positive argument and zero otherwise.

definition		definition	
biomass concentrations	$N_{\mathrm{wt}}(t), N_{\mathrm{wt}}(t)$	effective growth rate	$\bar{g}(R) = \frac{1-x}{Y_{\mathrm{wt}}/\bar{Y}} \cdot g_{\mathrm{wt}}(R) + \frac{x}{Y_{\mathrm{mut}}/\bar{Y}} g_{\mathrm{mut}}(R)$
initial mutant frequency	x		
extracellular resource conc.	$R(t)$	effective yield	$\bar{Y} = \left[\frac{1-x}{Y_{\mathrm{wt}}} + \frac{x}{Y_{\mathrm{mut}}}\right]^{-1}$
initial total biomass	N_0		
initial resource concentration	R_0	effective max. growth rate	$\bar{g}^{\max} = \frac{1-x}{Y_{\mathrm{wt}}/\bar{Y}} \cdot g_{\mathrm{wt}}^{\max} + \frac{x}{Y_{\mathrm{mut}}/\bar{Y}} \cdot g_{\mathrm{mut}}^{\max}$
population growth rates	$g_{\mathrm{wt}}(R), g_{\mathrm{mut}}(R)$		
biomass yields	$Y_{\mathrm{wt}}, Y_{\mathrm{mut}}$	critical concentration	$Z = K_{\mathrm{wt}}K_{\mathrm{mut}}\left[\frac{g_{\mathrm{wt}}^{\max}/\bar{g}^{\max}}{Y_{\mathrm{wt}}/\bar{Y}}\frac{1-x}{K_{\mathrm{wt}}} + \frac{g_{\mathrm{mut}}^{\max}/\bar{g}^{\max}}{Y_{\mathrm{mut}}/\bar{Y}}\frac{x}{K_{\mathrm{mut}}}\right]$
max. growth rates	$g_{\mathrm{wt}}^{\max}, g_{\mathrm{mut}}^{\max}$		
resource thresholds	$K_{\mathrm{wt}}, K_{\mathrm{mut}}$		

TABLE S2. **Key notation and definitions used in the model.** The subscripts "wt" and "mut" correspond to *wild-type* and *mutant*.

S2. NUMERICAL METHODS FOR BATCH DYNAMICS

It is not possible to analytically solve the ordinary differential equations for batch dynamics (Eq. (8)). To obtain explicit solutions to this model, we therefore numerically integrate the equations using the Scipy package [17]. We use the default Runge-Kutta algorithm "RK45" in the function `solve_ivp`. This interpolates the differential equation in fourth-order expansion over a short step size δt. The stepsize is automatically adjusted by `solve_ivp` to keep the error of integration below a threshold fixed by the user through the parameters `atol` and `rtol`. Our choice of `atol` $= 10^{-12}$ and `rtol` $= 10^{-8}$ is more restrictive than the default setting and ensures low errors on the state variables $N_{\mathrm{wt}}, N_{\mathrm{mut}}, R$.

The population dynamics in Eq. (8) reach the final equilibrium when all resources have been converted into biomass. This final equilibrium is the only attractor since the resources are finite and biomass is strictly increasing (no cell death); in particular, this system does not allow for limit cycles. However, the time to reach this equilibrium is infinite for all growth models in Table S1 (including the Monod model) except for the constant growth rate model. This is because the smooth decline of growth rate prevents full depletion of resources and allows populations to grow indefinitely at smaller but strictly positive growth rates. (The constant growth rate model allows for the same growth rate at arbitrarily low resource concentrations, which means the resources deplete to zero in finite time [1–3].)

For numerical calculations we must therefore set a finite saturation time t_{sat} such that the population dynamics are sufficiently close to their equilibrium state. We choose this time using the selection coefficient, which quantifies the relative change in the strain frequencies. Define the cumulative selection coefficient up to time t for a batch growth cycle as

$$s_t = \log\left(\frac{N_{\mathrm{mut}}(t)}{N_{\mathrm{wt}}(t)}\right) - \log\left(\frac{N_{\mathrm{mut}}(0)}{N_{\mathrm{wt}}(0)}\right). \tag{S3}$$

The total selection coefficient for the batch cycle is the cumulative selection coefficient in the limit of infinite time:

$$s = \lim_{t\to\infty} s_t. \tag{S4}$$

We want to define the saturation time t_{sat} as the time where the difference between the cumulative selection up to that time and the total selection is less than some tolerance. We can do this by determining an upper bound on the difference between total selection s and the selection at finite time t. As the population continues to grow after time t, the change in frequencies is bounded by the remaining available resources $R(t)$. The two possible extremes are if all remaining resources go to the wild-type,

in which case the biomass of the wild-type increases by $R(t)Y_{\text{wt}}$ and the mutant biomass remains constant, or if all remaining resources go to the mutant, in which case the biomass of the mutant increases by $R(t)Y_{\text{mut}}$ and the wild-type remains constant. Therefore the largest possible change in selection occurs in one of these two scenarios, and so the deviation in selection at time t from its equilibrium value is bounded by

$$|s_t - s| \leq \max\left\{ \log\left(1 + \frac{R(t)Y_{\text{mut}}}{N_{\text{mut}}(t)}\right), \log\left(1 + \frac{R(t)Y_{\text{wt}}}{N_{\text{wt}}(t)}\right) \right\}. \tag{S5}$$

We define the saturation time t_{sat} as the shortest time (infimum) such that the difference between the cumulative selection at that time and the total selection is smaller than a given error tolerance $\epsilon > 0$:

$$t_{\text{sat}} = \inf\left\{t > 0 : |s_t - s| < \epsilon\right\}. \tag{S6}$$

We implement this algorithmically by evaluating the simulation up to an initial time t, then evaluating the maximum future error on the selection coefficient from the right hand side of Eq. (S5), and then extending the simulation to $t + 10$ if the error exceeds a defined tolerance $\epsilon = 10^{-8}$. We iterate this process until the error is less than the threshold.

S3. RELATIONSHIP BETWEEN THE DILUTION FACTOR AND BOTTLENECK SIZE

Let superscript n refer to the dynamics during the nth batch growth cycle. The biomass at the beginning of $(n+1)$th cycle, $N_0^{(n+1)}$, equals the biomass at the end of the previous cycle n divided by the dilution factor $D^{(n)}$ for that cycle:

$$N_0^{(n+1)} = \frac{1}{D^{(n)}}\left(N_{\text{wt}}^{(n)}(t_{\text{sat}}) + N_{\text{mut}}^{(n)}(t_{\text{sat}})\right), \tag{S7}$$

where t_{sat} is the saturation time of the growth cycle. To determine the relationship with the bottleneck size of the previous growth cycle, we use the relationship between resource and biomass concentrations (Eq. (S1)) to show that at the end of the growth cycle, $R(t_{\text{sat}}) = 0$, and so

$$\begin{aligned} R^{(n)}(t_{\text{sat}}) &= 0 \\ &= R_0 + \frac{N_0^{(n)}}{\bar{Y}^{(n)}} - \frac{N_{\text{wt}}^{(n)}(t_{\text{sat}})}{Y_{\text{wt}}} - \frac{N_{\text{mut}}^{(n)}(t_{\text{sat}})}{Y_{\text{mut}}}. \end{aligned} \tag{S8}$$

Using this, we can insert the identity to obtain

$$\begin{aligned} N_0^{(n+1)} &= \frac{1}{D^{(n)}}\left(N_{\text{wt}}^{(n)}(t_{\text{sat}}) + N_{\text{mut}}^{(n)}(t_{\text{sat}})\right) \\ &= \frac{1}{D^{(n)}}\left(\frac{R_0 + \frac{N_0^{(n)}}{\bar{Y}^{(n)}}}{\frac{N_{\text{wt}}^{(n)}(t_{\text{sat}})}{Y_{\text{wt}}} + \frac{N_{\text{mut}}^{(n)}(t_{\text{sat}})}{Y_{\text{mut}}}}\right) \\ &\quad \times \left(N_{\text{wt}}^{(n)}(t_{\text{sat}}) + N_{\text{mut}}^{(n)}(t_{\text{sat}})\right) \\ &= \frac{1}{D^{(n)}}\left(R_0 + \frac{N_0^{(n)}}{\bar{Y}^{(n)}}\right)\left(\frac{1 - x^{(n+1)}}{Y_{\text{wt}}} + \frac{x^{(n+1)}}{Y_{\text{mut}}}\right)^{-1} \end{aligned} \tag{S9}$$

where we have used the fact that the frequencies of each strain at the end of the nth cycle equal their frequencies at the beginning of the $(n+1)$th cycle:

$$\frac{N_{\text{mut}}^{(n)}(t_{\text{sat}})}{N_{\text{wt}}^{(n)}(t_{\text{sat}}) + N_{\text{mut}}^{(n)}(t_{\text{sat}})} = x^{(n+1)}. \tag{S10}$$

Using the equation for the effective yield (Table S2), we obtain

$$N_0^{(n+1)} = \frac{1}{D^{(n)}}\left(R_0 + \frac{N_0^{(n)}}{\bar{Y}^{(n)}}\right)\bar{Y}^{(n+1)}. \tag{S11}$$

This establishes the general relationship between the bottleneck size and the dilution factor.

Under fixed-bottleneck batch dynamics $N_0^{(n)}$ is a fixed constant N_0, and so we can rearrange to determine how the dilution factor varies at each cycle:

$$D^{(n)} = \frac{R_0\bar{Y}^{(n+1)}}{N_0} + \frac{\bar{Y}^{(n+1)}}{\bar{Y}^{(n)}}. \tag{S12}$$

This shows that the dilution factor changes only if the strains have different yields, such that the effective yields $\bar{Y}^{(n)}$ change over cycles as the strain frequencies change. On the other hand, under fixed-dilution batch dynamics, $D^{(n)}$ is a fixed constant D, and Eq. (S11) simplifies to

$$N_0^{(n+1)} = \frac{1}{D}\left(R_0 + \frac{N_0^{(n)}}{\bar{Y}^{(n)}}\right)\bar{Y}^{(n+1)}. \tag{S13}$$

Under both serial transfer regimes, the steady state occurs when $D^{(n+1)} = D^{(n)}$, $N_0^{(n+1)} = N_0^{(n)}$, and $\bar{Y}^{(n+1)} = \bar{Y}^{(n)}$, which implies

$$D = \frac{R_0\bar{Y}}{N_0} + 1. \tag{S14}$$

This steady state occurs if 1) all strains have the same yields, such that the effective yield is constant; 2) one strain goes extinct; or 3) the two strains stably coexist.

S4. DEFINITION OF SELECTION COEFFICIENT

The instantaneous selection coefficient $\sigma(t)$ measures the rate of change in the logarithm of relative mutant frequency:

$$\sigma(t) = \frac{d}{dt} \log\left(\frac{N_{\text{mut}}(t)}{N_{\text{wt}}(t)}\right). \tag{S15}$$

This is a sufficient statistic for frequency change in the sense that knowledge of the instantaneous selection coefficient and the current mutant frequency is sufficient to predict the future mutant frequency over a short time horizon.

For population growth under batch dynamics, the repeated bottlenecks between growth cycles introduce randomness in the frequency trajectory of a mutant. We assume that this stochastic sampling at transfer dominates over the random fluctuations in individual birth rates within the growth cycle. Thus, the genetic drift in our model of serial transfer evolution occurs at the timescale of one growth cycle. To compare the strength of drift and selection on the same timescale, we integrate the instantaneous selection coefficient (Eq. (S15)) over time

$$s = \frac{1}{\Delta t} \int_0^{\Delta t} \sigma(t)\ \mathrm{d}t, \tag{S16}$$

where Δt is the length of the growth cycle. Note that the selection coefficient s is still defined as a rate per unit time and in the limit $\Delta t \to 0$ exactly matches the instantaneous selection coefficient (Eq. (S15)).

The selection coefficient s determines the change of frequency over multiple growth cycles. At the beginning of the nth cycle, the initial mutant frequency $x^{(n)}$ is given by

$$x^{(n)} = \frac{N_{\text{mut}}^{(n)}(0)}{N_{\text{mut}}^{(n)}(0) + N_{\text{wt}}^{(n)}(0)}, \tag{S17}$$

where $N_{\text{wt}}^{(n)}$ and $N_{\text{mut}}^{(n)}$ refer to the biomass of wild-type and mutant strain. The population grows to saturation, possibly experiences some frequency change, which sets the mutant frequency $x^{(n+1)}$ of the next cycle. This change is summarized by the selection coefficient

$$s^{(n)} = \log\left(\frac{x^{(n+1)}}{1 - x^{(n+1)}}\right) - \log\left(\frac{x^{(n)}}{1 - x^{(n)}}\right), \tag{S18}$$

which we compute from the integral definition (Eq. (S16)) using a timescale of $\Delta t = 1$ (per growth cycle). Knowledge of $s^{(n)}$ is sufficient to predict the initial mutant frequency in the next cycle

$$x^{(n+1)} = \frac{x^{(n)} \cdot \exp(s^{(n)})}{1 + x^{(n)} \cdot \left[\exp(s^{(n)}) - 1\right]}, \tag{S19}$$

assuming that the reduction of overall population size in the bottleneck does not affect mutant frequency. Thus, given the starting mutant frequency $x^{(1)}$ and the selection coefficients for each growth cycle $s^{(n)}$, the recursion in Eq. (S19) allows to predict the mutant trajectory without simulating the population dynamics within each growth cycle.

In general, the selection coefficients $\{s^{(n)}\}$ themselves depend on the initial mutant frequency $x^{(n)}$ of the growth cycle. Thanks to our explicit calculation of selection coefficients for the Monod model (see Eq. (4)), we can analyze this frequency dependence and find it to be negligible if mutations only affect the resource threshold, but not the maximum growth rate or biomass yield. In this case, we can calculate a single selection coefficient $s^{(1)}$ at invasion to predict over multiple cycles. We test this assumption in our simulations of trait evolution and observe that full frequency-dependence indeed does not affect the evolved resource threshold (compare Fig. S11).

S5. DERIVATION OF THE SELECTION COEFFICIENT FOR BATCH DYNAMICS

For populations growing in batch-culture, the selection coefficient reduces to the cumulative difference of growth rates:

$$s = \int_0^{\infty} \left[g_{\text{mut}}(R(t)) - g_{\text{wt}}(R(t))\right]\ \mathrm{d}t, \tag{S20}$$

where we have inserted the equations for mutant and wild-type growth from our model of populations dynamics (Eq. (8)) into the definition of s from Eq. (S16). The integral extends to infinite time for the growth dynamics to reach equilibrium (Sec. S2) so we therefore do not normalize by the time scale as in Eq. (S16); rather we leave it as understood that the selection coefficient is defined per growth cycle. We can change variables of the integral in Eq. (S20) from time t to resource concentration R:

$$s = \int_{R_0}^{0} \left[g_{\text{mut}}(R) - g_{\text{wt}}(R)\right] \cdot \frac{1}{\mathrm{d}R/\ \mathrm{d}t}\ \mathrm{d}R, \tag{S21}$$

where we have used the fact that R ranges from R_0 at the beginning of the growth cycle to 0 at the end of the growth cycle, and that R depends monotonically on t so that $dt/dR = (dR/dt)^{-1}$.

To compute this integral, we need to express the transient resource consumption rate dR/dt as an explicit function of current resource concentration R. As a first step, we rewrite the differential equation for resources into the product form

$$\frac{d}{dt}R(t) = -\frac{N_{\text{wt}}(t) + N_{\text{mut}}(t)}{\bar{Y}(t)} \cdot \left[\frac{1 - x(t)}{Y_{\text{wt}}/\bar{Y}(t)} g_{\text{wt}}(R) + \frac{x(t)}{Y_{\text{mut}}/\bar{Y}(t)} g_{\text{mut}}(R)\right], \tag{S22}$$

where we use the shorthand $\bar{Y}(t)$ for the time-dependent biomass yield (Table S2). This product separates into the joint biomass $N_{\rm wt}(t)+N_{\rm mut}(t)$ and a new parameter, that we term the *effective growth rate*:

$$\bar{g}(t,R) = \frac{1-x(t)}{Y_{\rm wt}/\bar{Y}(t)} g_{\rm wt}(R) + \frac{x(t)}{Y_{\rm mut}/\bar{Y}(t)} g_{\rm mut}(R). \quad \text{(S23)}$$

Equation (S22) suggests that this mean of wild-type and mutant growth rates acts as the effective growth rate of the joint population $N_{\rm wt}(t) + N_{\rm mut}(t)$. This effective growth rate is time-dependent due to underlying frequency change $x(t)$. Using this equation for the joint biomass (derived from Eq. (S1))

$$N_{\rm wt}(t) + N_{\rm mut}(t) = (R_0 - R(t)) \cdot \bar{Y}(t) + N_0 \frac{\bar{Y}(t)}{\bar{Y}}, \quad \text{(S24)}$$

we insert this and the equation for mean growth rate (Eq. (S23)) into Eq. (S21) for the selection coefficient:

$$s = \int_0^{R_0} \frac{g_{\rm mut}(R) - g_{\rm wt}(R)}{\bar{g}(t(R),R)} \cdot \frac{1}{N_0/\bar{Y}(t(R)) + R_0 - R} \, {\rm d}R. \quad \text{(S25)}$$

Equation (S25) is an exact expression but requires full knowledge of the resource trajectory $R(t)$ and its inverse $t(R)$. For a constant growth rate model (Table S1), this exact expression can be computed [1, 2]. However, for general growth models $g(R)$ and the Monod model in particular, the integral Eq. (S25) can only be solved under approximation. Previous work invoked the assumption of small initial mutant frequency $x \ll 1$ to replace mean growth rate and effective biomass yield by the wild-type traits [18, 19], but here we introduce a novel approximation that holds for all initial mutant frequencies.

We assume that the frequency-change over the growth cycle is small, such that the mean growth rate only depends on the resource concentration

$$\bar{g}(R) \approx \frac{1-x}{Y_{\rm wt}/\bar{Y}} g_{\rm wt}(R) + \frac{x}{Y_{\rm mut}/\bar{Y}} g_{\rm mut}(R), \quad \text{(S26)}$$

but not on time t. Similarly, we assume that the effective biomass yield remains close to the initial value: $\bar{Y}(t) \approx \bar{Y}$. Thus, we get the explicit integral formula for the selection coefficient:

$$s \approx \int_0^{R_0} \frac{g_{\rm mut}(R) - g_{\rm wt}(R)}{\frac{1-x}{Y_{\rm wt}/\bar{Y}} g_{\rm wt}(R) + \frac{x}{Y_{\rm mut}/\bar{Y}} g_{\rm mut}(R)} \cdot \frac{1}{N_0/\bar{Y} + R_0 - R} \, {\rm d}R, \quad \text{(S27)}$$

presented as Eq. (11) in the main text. This equation neglects the frequency-change $x(t)$ within the growth cycle, but still includes dependence on the initial mutant frequency x. One can show that the approximate integral in Eq. (S27) corresponds to first-order expansion of the exact integral (Eq. (S25) in terms of transient selection coefficients inside the growth cycle.

The exact selection coefficient in its integral form (Eq. (S25)) reveals generic properties of batch-culture competition. First, there is no direct selection for cell yield. A mutant with higher efficiency $Y_{\rm mut}$ but equal growth response is neutral. Thus with uncorrelated mutation supply, we expect cell yield to evolve neutrally [3, 20]. Second, the selection on the growth rate function $g(R)$ is distributed unequally across concentrations. In the integrand of Eq. (S25), the difference in growth rates at each resource concentration R is weighted by the *fold-change spectrum* $1/(N_0/\bar{Y} + R_0 - R)$. This weight peaks at the initial resource concentration R_0 (see Fig. S18A) and is independent of the growth rate model $g(R)$. For growth cycles with large fold-change ($R_0 Y/N_0 \gg 1$), the selection coefficient s roughly corresponds to the growth rate difference at initial concentrations because most generations occur at near-constant concentrations close to R_0 (compare Fig. S18B).

The approximate selection coefficient Eq. (S27) shows that selection only acts on ratios of growth rates, since the growth rates appear in both the numerator and denominator of the integrand. The dependence on growth rate ratios means that alternative growth models can still lead to equivalent selection on traits. For example, if we take any growth rate models from Table S1, if the mutant and wild-type differ only in their maximum growth rates $g^{\rm max}$ (but not other parameters such as K), then their selection coefficients will depend only on the ratio $g^{\rm max}_{\rm mut}/g^{\rm max}_{\rm mut}$ and not other details of the specific model.

S6. CALCULATION OF THE SELECTION COEFFICIENT FOR THE MONOD MODEL

In this section, we apply the integral formula Eq. (S27) to calculate the selection coefficient for a wild-type and mutant strain computing under the Monod model. Let

$$\Delta g^{\rm max} = g^{\rm max}_{\rm mut} - g^{\rm max}_{\rm wt}, \quad \Delta K = K_{\rm mut} - K_{\rm wt}, \quad \text{(S28)}$$

denote the absolute trait difference in maximum growth rate and resource threshold. First, we rewrite the relative growth rate difference

$$\frac{g_{\rm mut}(R) - g_{\rm wt}(R)}{\bar{g}(R)} = \frac{\Delta g^{\rm max}}{\bar{g}^{\rm max}} - \frac{\Delta K}{R+Z} \cdot \frac{g^{\rm max}_{\rm wt} g^{\rm max}_{\rm mut}}{\bar{g}^{\rm max} \bar{g}^{\rm max}}, \quad \text{(S29)}$$

using the effective maximum growth rate

$$\bar{g}^{\rm max} = \frac{1-x}{Y_{\rm wt}/\bar{Y}} \cdot g^{\rm max}_{\rm wt} + \frac{x}{Y_{\rm mut}/\bar{Y}} \cdot g^{\rm max}_{\rm mut}, \quad \text{(S30)}$$

and the critical resource concentration

$$Z = K_{\mathrm{wt}} K_{\mathrm{mut}} \cdot \Big[\frac{g_{\mathrm{wt}}^{\max}/\bar{g}^{\max}}{Y_{\mathrm{wt}}/\bar{Y}} \cdot \frac{1-x}{K_{\mathrm{wt}}} + \frac{g_{\mathrm{mut}}^{\max}/\bar{g}^{\max}}{Y_{\mathrm{mut}}/\bar{Y}} \cdot \frac{x}{K_{\mathrm{mut}}} \Big] \tag{S31}$$

as effective traits of the joint population to simplify the notation (Table S2). The separation between maximum growth rate and resource threshold in Eq. (S29) leads to distinct components of the selection coefficient:

$$s \approx s_{\mathrm{high}} + s_{\mathrm{low}} \tag{S32a}$$

where

$$s_{\mathrm{high}} = \frac{\Delta g^{\max}}{\bar{g}^{\max}} \cdot \log\left(1 + \frac{R_0 \bar{Y}}{N_0}\right) \tag{S32b}$$

$$s_{\mathrm{low}} = \frac{-\Delta K}{R_0 + N_0/\bar{Y} + Z} \frac{g_{\mathrm{wt}}^{\max}}{\bar{g}^{\max}} \frac{g_{\mathrm{mut}}^{\max}}{\bar{g}^{\max}} \cdot \log\left(\left(1 + \frac{R_0 \bar{Y}}{N_0}\right)\left(1 + \frac{R_0}{Z}\right)\right). \tag{S32c}$$

Here we describe the selection coefficient in terms of absolute trait differences between mutant and wild-type straits. Assuming a relative effect of mutation on both traits as in Eq. (3), we recover the formulation shown as Eq. (4) in the main text.

The formula for the selection coefficient is based on an approximation of small frequency change. In Fig. S16 we compare the approximate selection coefficient against the exact selection coefficient obtained from numerically solving the differential equation. The simulations show that the approximate selection coefficient is accurate up to large values of order $s \approx 1$. This means that, while we mainly consider the scenario of weak selection ($|s| < 1$), the approximation is excellent even when selection is strong. Intuitively, the approximation breaks down because of wrongly estimating the mean resource consumption rate which we expect to prominent when the yields and realized growth rates differ strongly between the two strains.

We briefly discuss an interpretation for the parameter Z. The instantaneous selection coefficient (Eq. (S15)) within the batch culture growth cycle

$$\sigma(t) = g_{\mathrm{mut}}(R(t)) - g_{\mathrm{wt}}(R(t)), \tag{S33}$$

can be decomposed into two components

$$\sigma = \sigma_{\max} + \sigma_{\mathrm{lin}}, \tag{S34a}$$

where

$$\sigma_{\max} = \Delta g^{\max} \cdot \frac{R}{R + K_{\mathrm{wt}}} \frac{R}{R + K_{\mathrm{mut}}} \tag{S34b}$$

$$\sigma_{\mathrm{lin}} = \Delta a \cdot R \cdot \frac{K_{\mathrm{wt}}}{R + K_{\mathrm{wt}}} \frac{K_{\mathrm{mut}}}{R + K_{\mathrm{mut}}}. \tag{S34c}$$

Here we introduce the *linear growth rate* $a = g^{\max}/K$ as a shorthand of notation. The first component $\sigma_{\max}$ quantifies growth rate difference at excess conditions, where both strains grow close to their maximum growth rates. The second component σ_{lin} measures growth rate differences in the opposite regime, where both strains grow below their resource thresholds. The relative size of the two components varies shifts with resource concentration and also depends on the mutation effect on maximum growth rate and resource threshold, here expressed in Δa.

The effective parameter Z acts as an intrinsic scale in the resource dependence. Normalizing for different relative mutation effects, both components contribute equally to growth rate difference exactly at external concentration $R = Z$ such that

$$\frac{\sigma_{\max}(Z)}{\Delta g^{\max}/\bar{g}^{\max}} = \frac{\sigma_{\mathrm{lin}}(Z)}{\Delta a/\bar{a}}, \tag{S35}$$

where the effective linear growth rate $\bar{a}$ is defined (in analogy with the effective maximum growth rate defined in Eq. (S30)) as

$$\bar{a} = \frac{1-x}{Y_{\mathrm{wt}}/\bar{Y}} \cdot \frac{g_{\mathrm{wt}}^{\max}}{K_{\mathrm{wt}}} + \frac{x}{Y_{\mathrm{mut}}/\bar{Y}} \cdot \frac{g_{\mathrm{mut}}^{\max}}{K_{\mathrm{mut}}}. \tag{S36}$$

This means, at concentration Z both components of the growth rate difference in Eq. (S34) receive equal selection pressure.

The decomposition in Eq. (S34) more generally suggests an alternative parametrization of the Monod model and its selection coefficient. We can replace the resource threshold K by the linear growth rate $a = g^{\max}/K$. This alternative trait corresponds to the growth rate in the limit of low resource concentrations where the Monod model behaves linearly (see Sec. S1). The selection coefficient in Eq. (S32) can be rewritten as

$$s \approx s_{\max} + s_{\mathrm{lin}}, \tag{S37a}$$

where

$$s_{\max} = \frac{\Delta g^{\max}}{\bar{g}^{\max}} \cdot \Big[\frac{R_0 + N_0/\bar{Y} - Z}{R_0 + N_0/\bar{Y} + Z} \cdot \log\left(1 + \frac{R_0 \bar{Y}}{N_0}\right) \Big], \tag{S37b}$$

$$s_{\mathrm{lin}} = \frac{\Delta a}{\bar{a}} \cdot \Big[\frac{Z}{R_0 + N_0/\bar{Y} + Z} \cdot \log\left(1 + \frac{R_0 \bar{Y}}{N_0}\right)\left(1 + \frac{R_0}{Z}\right) \Big]. \tag{S37c}$$

The selection coefficient maps the life-history traits to relative fitness and the parametrization in a is well-suited to study the structure of this map under environmental variation. In the limit of high nutrient concentrations,

the total resources are large compared to the critical concentration Z. The selection coefficient then reduces to the component of maximum growth:

$$s \approx s_{\max} \qquad \text{as } R_0 \to \infty. \tag{S38}$$

In the opposite limit, the selection coefficient only acts on the growth rate at low concentrations. In this sense, the selection coefficient recovers the limiting behaviour of the underlying growth response:

$$s \approx s_{\text{lin}} \qquad \text{as } R_0 \to 0. \tag{S39}$$

This means that g and a are the marginal traits that exclusively control growth in the limiting environments. The selection coefficient reduces to one component or the other. For the parametrization based on K given below, this is not true — both g and K contribute at low concentrations.

S7. DERIVATION OF SELECTION COEFFICIENT FOR CHEMOSTAT

For a population in chemostat conditions (Eq. (10)), the instantaneous selection coefficient $\sigma(t)$ (Eq. (S15)) only depends on the difference in growth rates. At a given resource concentration $R(t)$, this growth rate difference can be decomposed in to two trait components

$$\sigma \approx \sigma_{\text{high}} + \sigma_{\text{low}}, \tag{S40a}$$

where

$$\sigma_{\text{high}} = \frac{\Delta g^{\max}}{\bar{g}^{\max}} \cdot \bar{g}(R), \tag{S40b}$$

$$\sigma_{\text{low}} = \frac{-\Delta K}{R+Z} \frac{g_{\text{wt}}^{\max}}{\bar{g}^{\max}} \frac{g_{\text{mut}}^{\max}}{\bar{g}^{\max}} \cdot \bar{g}(R). \tag{S40c}$$

We can derive this by multiplying Eq. (S29) with the mean growth rate for the Monod model

$$\begin{aligned} \bar{g}(R) =& \bar{g}^{\max} \cdot \frac{R}{R+K_{\text{wt}}} \frac{R}{R+K_{\text{mut}}} \\ &+ \bar{a} \cdot R \cdot \frac{K_{\text{wt}}}{R+K_{\text{wt}}} \frac{K_{\text{mut}}}{R+K_{\text{mut}}}. \end{aligned} \tag{S41}$$

The two components σ_{high} and σ_{low} are consistent with our results for batch culture conditions (Eq. (S32)). By integrating the instantaneous component σ_{high} over the growth cycle, we recover the component s_{high} for batch-culture growth.

We assume a specific scenario for selection in chemostat populations, where mutants arise at small frequency x on top of a wild-type population. This is plausible if mutations occur not too frequently, such that the chemostat population is replaced by a mutant and reaches the new steady state before the next mutation arises. A chemostat population in steady-state drives the media concentration to the critical value

$$R^* = K_{\text{wt}} \cdot \frac{d}{g_{\text{wt}}^{\max} - d}, \tag{S42}$$

where cell growth rate matches the dilution factor $g_{\text{wt}}(R^*) = d$ [21]. After the mutant appears, the resource concentration $R(t) \approx R^*$ remains constant over a short timespan while the mutant still has low frequency $x \ll 1$. In this timewindow, the mean growth rate Eq. (S41) is set by the wild-type only and thus, equals the dilution rate

$$\bar{g}(R^*) \approx d. \tag{S43}$$

We insert Eq. (S42) and Eq. (S43) into Eq. (S40) to calculate the selection coefficient at invasion with small mutant frequency $x \ll 1$

$$\sigma_{\text{high}} = \frac{\Delta g^{\max}}{g_{\text{wt}}^{\max}} \cdot d \tag{S44a}$$

$$\begin{aligned} \sigma_{\text{low}} =& \frac{-\Delta K}{(-\Delta K) \cdot d + K_{\text{mut}} \cdot g_{\text{wt}}^{\max}} \cdot \frac{g_{\text{mut}}^{\max}}{g_{\text{wt}}^{\max}} \\ &\cdot (g_{\text{wt}}^{\max} - d) d. \end{aligned} \tag{S44b}$$

Equation (S44) is mathematically equivalent to Eq. (5), which we have rewritten in terms of relative mutation effects $\kappa = \Delta K / K$ and $\gamma = \Delta g^{\max} / g^{\max}$. Assuming this relative mutation effect κ, the selection on resource threshold σ_{low} is independent of the background trait and thus does not achieve selection-drift balance (compare Fig. S9 for batch culture). This has been observed independently in calculations by Dykhuizen et al. [22], who similarly decompose the growth rate difference in chemostats. Again, the chemostat selection coefficient in Eq. (S44) can be rewritten in terms of the linear growth rate $a = g^{\max}/K$ instead of the resource threshold K.

S8. DEPENDENCE OF SELECTION ON RESOURCE CONCENTRATION

In this section, we use the explicit formula for s in batch culture (Eq. (S32)) to describe how selection varies with the initial resource concentration R_0 of the growth cycle. For fixed initial biomass N_0, there is an optimum concentration that maximizes the selection on the resource threshold K. Figure S6A shows non-monotonic behaviour of s_{low} with resource concentration for an example mutation with beneficial effect both on maximum growth rate $g^{\max}$ and resource threshold K. In particular, this optimum does not rely on a trade-off between the two traits. Instead, Fig. S6B demonstrates that s_{low} is the product of two opposing forces: the overall budget

for selection in the growth cycle (equivalent to number of generations) increases with R_0, but the relative selection pressure on the resource threshold decreases. We can identify these two factors from Eq. (S32c) for s_{low} on the resource threshold: the selection coefficient is the product of a trait term

$$s_{\text{low}} \propto \frac{-\Delta K}{R_0 + N_0/\bar{Y} + Z} \frac{g_{\text{wt}}^{\max}}{\bar{g}^{\max}} \frac{g_{\text{mut}}^{\max}}{\bar{g}^{\max}}, \tag{S45}$$

and a logarithmic term

$$s_{\text{low}} \propto \log\left(\left(1 + \frac{R_0\bar{Y}}{N_0}\right)\left(1 + \frac{R_0}{Z}\right)\right), \tag{S46}$$

which increases directly with the number of generations of growth in the growth cycle. The optimum concentration, in general, is determined by the wild-type resource threshold (compare Fig. S6C). On evolutionary timescales, Fig. S6D shows that the overall speed of adaptation has a local minimum over resource concentrations. Intuitively, the non-monotonic selection on resource threshold causes the distribution of fitness effects (DFE) to vary in width, which is a key determinant of the speed of adaption [23].

These effects are not observed in batch dynamics with fixed-dilution factor, where selection s_{low} decreases strictly monotonically with resource concentration. The same example mutation in Fig. S7 reaches peak selection at the lowest nutrient concentration R_0. Intuitively, the fixed dilution factor D means the total budget for selection (number of generations) is independent of the initial concentration R_0 and low concentrations mean a larger fraction of time spent in deceleration, but not less generations.

S9. DERIVATION OF SELECTION-DRIFT BALANCE CONDITION

We can map the dynamics of the mutant frequency over batch growth cycles to the Wright-Fisher model of population genetics, where each batch growth cycle corresponds to discrete time step [1, 24]. First, we assume the mutation arises only at the beginning of the growth cycle at frequency $1/N_0$, where N_0 is the bottleneck population size measured in number of cells. Let $s(x)$ be the selection coefficient for the mutant over a whole batch growth cycle, with explicit dependence on the frequency x of the mutant at the beginning of the cycle. In the limit of large population size ($N_0 \gg 1$) and weak selection ($|s(x)| \ll 1$), the fixation probability for the mutant is [25]

$$p(s) = \frac{\int_0^{1/N_0} \exp\left(-2N_0 \int_0^x s(y)\,\mathrm{d}y\right)\,\mathrm{d}x}{\int_0^1 \exp\left(-2N_0 \int_0^x s(y)\,\mathrm{d}y\right)\,\mathrm{d}x}. \tag{S47}$$

However, if the selection coefficient $s(x)$ is approximately constant over mutant frequencies x, we can simplify this to

$$p(s) = \frac{1 - e^{-2s}}{1 - e^{-2N_0 s}}. \tag{S48}$$

In the limit of weak selection ($s \ll 1$), we can expand Eq. (S48) to leading order in s:

$$p(s) \approx \frac{1}{N_0} + \left(1 - \frac{1}{N_0}\right) s, \tag{S49}$$

where the first term captures the probability of fixation due purely to demographic fluctuations (genetic drift), while the second term captures the correction due to selection. The balance between selection and drift therefore occurs when these two contributions are approximately equal, which gives us $s \approx 1/N_0$ (Eq. (6) from the main text) under the additional assumption that N_0 is large.

Now we consider the effect of a mutation arising at some intermediate time t during a growth cycle. Since at this time there are $N_{\text{wt}}(t)$ wild-type cells, the initial frequency of the mutant is $1/N_{\text{wt}}(t)$, and the amount of remaining resources is $R(t) = R_0 - (N_{\text{wt}}(t) - N_{\text{wt}}(0))/Y_{\text{wt}}$. Therefore the frequency of the mutant at the end of this cycle is

$$x(t) = \frac{e^{s(t)}}{e^{s(t)} + N_{\text{wt}}(t) - 1}, \tag{S50}$$

where $s(t)$ is the selection coefficient for this mutant, assuming a growth cycle that starts when the mutation arises (so we use $R(t)$ as the initial amount of resources and $N_{\text{wt}}(t)$ as the initial population size).

Let $p(t)$ be the probability that this mutant ultimately fixes. This is the probability that n mutant cells survive the transfer, multiplied by the probability those mutants fix, averaged over all possible n:

$$\begin{aligned}
p(t) =& \sum_{n=0}^{N_0} \binom{N_0}{n} (x(t))^n (1 - x(t))^{N_0 - n} \left(\frac{1 - e^{-2ns(0)}}{1 - e^{-2N_0 s(0)}}\right) \\
\approx& \sum_{n=0}^{N_0} \binom{N_0}{n} (x(t))^n (1 - x(t))^{N_0 - n} \\
&\times \left(\frac{n}{N_0} + n\left(1 - \frac{n}{N_0}\right) s(0)\right) \\
=& x(t)\left[1 + (N_0 - 1)s(0)(1 - x(t))\right] \\
\approx& \frac{1}{N_{\text{wt}}(t)} + \left(\frac{N_0 - 1}{N_{\text{wt}}(t)}\right)\left(\frac{N_{\text{wt}}(t) - 1}{N_{\text{wt}}(t)}\right) s(0) \\
&+ \left(\frac{N_{\text{wt}}(t) - 1}{[N_{\text{wt}}(t)]^2}\right) s(t),
\end{aligned} \tag{S51}$$

where we have invoked the weak-selection approximation to the fixation probability (Eq. (S49)) on the second line, evaluated moments of the binomial distribution on the third line, and then expanded the frequency $x(t)$ (Eq. (S50)) to leading order in $s(t)$ on the last line. By neglecting terms that are higher-order in $1/N_{\rm wt}(t)$ and $s(t)$, we obtain

$$p(t) \approx \frac{1}{N_{\rm wt}(t)} + \left(\frac{N_0 - 1}{N_{\rm wt}(t)}\right) s(0). \tag{S52}$$

Note that this only depends on the selection coefficient of the mutant starting at the beginning of the cycle; to leading order there is no dependence on the selection coefficient during that first cycle $s(t)$. If we calculate the condition for selection-drift balance as before, we obtain $s(0) \approx 1/N_0$ as before. That is, the dependence on the wild-type population size at which the mutant first arises $N_{\rm wt}(t)$ is irrelevant to the selection-drift balance. Therefore mutations arising during growth cycles have no effect on the selection-drift balance condition to leading order.

S10. THE EVOLVED RESOURCE THRESHOLD AT SELECTION-DRIFT BALANCE

In this section, we calculate the evolved resource threshold $K_{\rm evo}$ as a function of environmental concentration R_0 and effective population size $N_{\rm e}$. We assume mutations have a relative effect κ on the resource threshold, but no effect on maximum growth rate or biomass yield. The sign and absolute value of κ can vary from mutant to mutant, as we do in our simulations, but we assume that there is a maximum possible value $|\kappa_{\rm max}|$ for beneficial mutations that reduce K. Intuitively, this means that a single mutation cannot lower the trait by more than a fixed percentage $|\kappa_{\rm max}|$.

The maximum possible selection coefficient for any mutant on the background of a wild-type trait K is thus

$$\begin{aligned} s_{\rm low} =& |\kappa_{\rm max}| \left(\frac{\frac{K}{R_0}}{(1+\kappa_{\rm max})\frac{K}{R_0} + 1 + \frac{N_0}{R_0 Y}} \right) \\ & \cdot \log\left[\left(1 + \frac{R_0 Y}{N_0}\right) \left(1 + \frac{1}{(1+\kappa_{\rm max})\frac{K}{R_0}}\right) \right], \end{aligned} \tag{S53}$$

where we have rewritten the selection coefficient (Eq. (S32)) in terms of the ratio K/R_0 between background trait and initial resource concentration. Note that we write Y for the wild-type biomass yield, which remains unchanged throughout evolution.

To simplify Eq. (S53), we assume that the maximum mutation effect is small ($|\kappa_{\rm max}| \ll 1$), the value of the threshold K relative the initial resource concentration is small ($K/R_0 \ll 1$), and the fold-change over the growth cycle is large ($R_0 Y/N_0 \gg 1$). This is true for growth cycles in typical laboratory evolution experiments, with typical dilution factors between $D = 100$ [26] and $D = 1500$ [27]. We therefore approximate the selection coefficient in Eq. (S53) by keeping only leading-order terms in these parameters:

$$s_{\rm low} \approx |\kappa_{\rm max}| \frac{K}{R_0} \log\left(\frac{R_0 Y/N_0}{K/R_0}\right). \tag{S54}$$

The evolved threshold $K_{\rm evo}$ is defined as the value of the threshold K such that the selection coefficient for a mutation on this threshold equals the fixation probability of a neutral mutation. We must therefore also assume that the maximum strength of selection, which occurs for large K, is greater than the neutral fixation probability (Fig. S9). In the limit of small $|\kappa_{\rm max}|$ and large $R_0 Y/N_0$, the maximum selection coefficient is $|\kappa_{\rm max}| \log(R_0 Y/N_0)$, and so this must be greater than $1/N_{\rm e}$. To solve for $K_{\rm evo}$, we then set the selection coefficient in Eq. (S54) equal to $1/N_{\rm e}$ (using Eq. (6)) and solve to obtain

$$K_{\rm evo} \approx -\frac{R_0}{N_{\rm e}|\kappa_{\rm max}| W_{-1}\left(-\frac{1}{N_{\rm e}|\kappa_{\rm max}| R_0 Y/N_0}\right)}, \tag{S55}$$

where $W_{-1}(z)$ is the -1 branch of the Lambert W function, defined as the solution of the equation $ye^y = z$ for $-e^{-1} \le z < 0$ (e denotes Euler's constant). The latter condition is met since the argument of the W function, $-1/(N_{\rm e}|\kappa_{\rm max}| R_0 Y/N_0)$ is certainly less than zero, but also

$$\begin{aligned} -\frac{1}{N_{\rm e}|\kappa_{\rm max}| R_0 Y/N_0} \ge& -\frac{1}{N_{\rm e}|\kappa_{\rm max}| e \log(R_0 Y/N_0)} \\ >& -\frac{1}{e}, \end{aligned} \tag{S56}$$

where on the first line we have used the fact that $e\log(R_0 Y/N_0) \le R_0 Y/N_0$ and on the second line we have used $N_{\rm e}|\kappa_{\rm max}| \log(R_0 Y/N_0) > 1$ from our previous assumption that the maximum strength of selection is bigger than genetic drift. We can further simplify Eq. (S55) using the approximation $W_{-1}(z) \approx \log(-z)$ for $|z| \ll 1$, which gives us Eq. (7) in the main text.

S11. INFERRING RESOURCE THRESHOLDS FROM GROWTH CURVE DECELERATION

Measuring the resource threshold K requires observations of deceleration. Here we show that for the typical conditions found in optical plate reader measurements, the biomass fold-change in deceleration is below the detection limit.

Figure S12 shows the monoculture growth curve of an example strain, such that the resource threshold K is of the same order as the initial resource concentration of the growth cycle. This condition provides sufficient

datapoints in both steady exponential growth (used to fit $g^{\max}$) and deceleration (used to fit K). Intuitively, this last phase of growth holds most information on the resource threshold. Detailed analysis in the 1980s describes this as a problem of statistical estimation, calculating parameter sensitivities to identify the optimum measurement concentration ($K/R_0 \approx 1$) and discussing variable transformations to simplify the regression (see Robinson [28] for an overview).

However, our predictions for the evolved resource threshold K_{evo} means that this estimate is always ill-posed when populations are observed in the concentration of their natural habitat or higher. Along the growth curve, we define the onset of deceleration t_{decel} as

$$N(t_{\text{decel}}) = N_0 + (R_0 - K)Y, \tag{S57}$$

where the remaining resources exactly match the resource threshold K. The growth curve continues to saturation eventually, and the fold-change in this last window of growth is given by the ratio

$$\frac{N(t_{\text{sat}})}{N(t_{\text{decel}})} = 1 + \frac{\frac{K}{R_0}}{(1 - \frac{K}{R_0}) + \frac{N_0}{R_0 Y}}, \tag{S58}$$

which still depends on the total fold-change of the growth cycle. We make two approximations: the overall biomass fold-change is expected to be large such that $R_0 Y/N_0 \gg 1$ and the resource threshold is small compared to the concentration such that $K/R_0 \ll 1$. This is plausible for phenotypic assays of *E. coli* on glucose with concentrations ($0.2\% \approx 10$ mM) which is much higher than the resource threshold of *E. coli* isolates (see Fig. 2B). Growth curves in this scenario show an approximate fold-change

$$\frac{N(t_{\text{sat}})}{N(t_{\text{decel}})} \approx 1 + \frac{K}{R_0}, \tag{S59}$$

from the onsset of deceleration to saturation.

The limited sensitivity of plate reader instruments mean that only differences in optical density greater than the detection limit $\Delta OD \approx 0.01 - 0.001$ can be resolved. Equation (S59) indicates that the observable difference is much smaller for an evolved population. To see this, assume that biomass at saturation roughly reaches $N(t_{\text{sat}}) \approx 1$ in units of optical density. The increment in optical density over the deceleration is proportional to K_{evo}/R_0, which scales with the effective population size (see Eq. (S55)). The estimated effective population size $N_{\text{e}} \approx 10^8 - 10^9$ for bacteria in the wild [29] leads to late deceleration and OD increments much below the sensitivity ΔOD of common plate readers.

Intuitively, the adaptation of the resource threshold changes the growth curve shape. The ratio between resource threshold of the strain and initial concentration determines the curvature at the end of the growth curve. Evolved population at selection-drift balance shows a sharp arrest in the concentration of their habitat. The smooth shape only is revealed at lower concentrations, however, these often shrink the absolute growth below the minimum optical density that can be detected.

[1] Michael Manhart, Bharat V. Adkar, and Eugene I. Shakhnovich. Trade-offs between microbial growth phases lead to frequency-dependent and non-transitive selection. *Proceedings of the Royal Society B: Biological Sciences*, 285(1872):20172459, February 2018. Publisher: Royal Society.

[2] M. Manhart and E. I. Shakhnovich. Growth tradeoffs produce complex microbial communities on a single limiting resource. *Nat Commun*, 9:3214, 2018.

[3] Jie Lin, Michael Manhart, and Ariel Amir. Evolution of Microbial Growth Traits Under Serial Dilution. *Genetics*, May 2020. Publisher: Genetics Section: Investigation.

[4] R. H. MacArthur. Species packing and competitive equilibria for many species. *Theor Pop Biol*, 1:1–11, 1970.

[5] F. F. Blackman. Optima and limiting factors. *Annals of Botany*, 19:281–295, 1905.

[6] J. R. Casey and M. J. Follows. A steady-state model of microbial acclimation to substrate limitation. *PLoS Comput Biol*, 16:e1008140, 2020.

[7] C. S. Holling. Some characteristics of simple types of predation and parasitism i. *The Canadian Entomologist*, 91:358–369, 1959.

[8] J. Monod. The growth of bacterial cultures. *Annu Rev Microbiol*, 3:371–394, 1949.

[9] M. R. Droop. Some thoughts on nutrient limitation in algae. *Journal of Phycology*, 9:264–272, 1973.

[10] U. Sommer. A comparison of the droop and the monod models of nutrient limited growth applied to natural populations of phytoplankton. *Funct Ecol*, 5:535–544, 1991.

[11] W. G. Sunda, K. W. Shertzer, and D. R. Hardison. Ammonium uptake and growth models in marine diatoms: Monod and Droop revisited. *Mar Ecol Prog Ser*, 386:29–41, 2009.

[12] H. Wang, P. V. Garcia, S. Ahmed, and C. M. Heggerud. Mathematical comparison and empirical review of the Monod and Droop forms for resource-based population dynamics. *Ecol Model*, 466:109887, 2022.

[13] L. Von Bertalanffy. Quantitative laws in metabolism and growth. *Q Rev Biol*, 32:217–231, 1957.

[14] E. Sperfeld, D. Martin-Creuzburg, , and A. Wacker. Multiple resource limitation theory applied to herbivorous consumers: Liebig's minimum rule vs. interactive co-limitation. *Ecol Lett*, 15:142–150, 2012.

[15] H. Moser. *The Dynamics of Bacterial Populations Maintained in the Chemostat.* Carnegie Institution of Washington, 1958.

[16] S. F. M. Hart, D. Skelding, A. J. Waite, J. C. Burton, and W. Shou. High-throughput quantification of microbial birth and death dynamics using fluorescence microscopy. *Quant Biol*, 7:69–81, 2019.

[17] Pauli Virtanen, Ralf Gommers, Travis E. Oliphant, Matt Haberland, Tyler Reddy, David Cournapeau, Evgeni

Burovski, Pearu Peterson, Warren Weckesser, Jonathan Bright, Stéfan J. van der Walt, Matthew Brett, Joshua Wilson, K. Jarrod Millman, Nikolay Mayorov, Andrew R. J. Nelson, Eric Jones, Robert Kern, Eric Larson, C J Carey, İlhan Polat, Yu Feng, Eric W. Moore, Jake VanderPlas, Denis Laxalde, Josef Perktold, Robert Cimrman, Ian Henriksen, E. A. Quintero, Charles R. Harris, Anne M. Archibald, Antônio H. Ribeiro, Fabian Pedregosa, Paul van Mulbregt, and SciPy 1.0 Contributors. SciPy 1.0: Fundamental Algorithms for Scientific Computing in Python. *Nature Methods*, 17:261–272, 2020.

[18] Frank M. Stewart and Bruce R. Levin. Partitioning of Resources and the Outcome of Interspecific Competition: A Model and Some General Considerations. *The American Naturalist*, 107(954):171–198, March 1973. Publisher: The University of Chicago Press.

[19] Meike T. Wortel. Evolutionary coexistence in a fluctuating environment by specialization on resource level. Technical report, September 2021. Company: Cold Spring Harbor Laboratory Distributor: Cold Spring Harbor Laboratory Label: Cold Spring Harbor Laboratory Section: New Results Type: article.

[20] Farida Vasi, Michael Travisano, and Richard E. Lenski. Long-Term Experimental Evolution in Escherichia coli. II. Changes in Life-History Traits During Adaptation to a Seasonal Environment. *The American Naturalist*, 144(3):432–456, September 1994.

[21] D. Tilman. *Resource competition and community structure*. Princeton University Press, Princeton, NJ, 1982.

[22] Daniel Dykhuizen and Daniel Hartl. Evolution of competitive ability in escherichia coli. *Evolution*, 35:581, 1981.

[23] M. M. Desai, D. S. Fisher, and A. W. Murray. The speed of evolution and maintenance of variation in asexual populations. *Curr Biol*, 17:385–394, 2007.

[24] J. F. Crow and M. Kimura. *An Introduction to Population Genetics Theory*. Harper and Row, New York, 1970.

[25] Motoo Kimura. On the Probability of Fixation of Mutant Genes in a Population. *Genetics*, 47(6):713–719, June 1962. Publisher: Genetics Section: INVESTIGATIONS.

[26] R. E. Lenski, M. R. Rose, S. C. Simpson, and S. C. Tadler. Long-term experimental evolution in Escherichia coli. I. Adaptation and divergence during 2,000 generations. *Am Nat*, 138:1315–1341, 1991.

[27] Nittay Meroz, Nesli Tovi, Yael Sorokin, and Jonathan Friedman. Community composition of microbial microcosms follows simple assembly rules at evolutionary timescales. *Nature Communications*, 12, 2021.

[28] Joseph A.Robinson. Determining microbial kinetic parameters using nonlinear regression analysis. *Advances in Microbial Ecology*, 8:61–114, 1985.

[29] Louis-Marie Bobay and Howard Ochman. Factors driving effective population size and pan-genome evolution in bacteria. *BMC Evolutionary Biology*, 18:153, October 2018.